ABSTRACT

LEE, HOON JOO. Design and Development of Superhydrophobic Textile Surfaces. (Under the direction of Stephen Michielsen and Trevor J. Little).

The relationship between contact angles, surface tensions and surface roughness is reviewed. The various numerical formulae related to contact angles were used to predict the surface tension and wetting behavior of polymer surfaces. The apparent contact angle of a droplet deposited on a textured surface is presented, and the characteristics required for a superhydrophobic surface are described.

The numerical formulae related to superhydrophilic and superhydrophobic polymer rough surfaces are shown using two approaches, Wenzel and Cassie-Baxter models. Using these models as a guide, artificial superhydrophilic or superhydrophobic surfaces were created. Rough nylon surfaces mimicking the Lotus leaf were created by coating polyester surface with nylon 6,6 short fibers using the flocking process. Poly(acrylic acid) (PAA) chains were grafted onto nylon 6,6 surfaces followed by grafting 1H, 1H-perfluorooctylamine to the PAA chains. Water contact angles as high as 178º were achieved.

For a woven superhydrophobic surface, the original Cassie-Baxter model better describes the wetting of rough surfaces. Using topological and chemical surface modification of nylon 6,6 woven fabric, artificial Lotus leaves having water contact angles as high as 168° were prepared. Good agreement between the predictions based on the original Cassie-Baxter model and experiments was obtained. However, the version of the Cassie-Baxter

model in current use could not explain the wetting behavior of woven fabrics since the surface area fractions in this form is valid only when the liquid is in contact with a flat porous surface.

The angle at which a water droplet rolls off the surface has also been used to define a superhydrophobic surface. It is shown that the roll-off angle is highly dependent on droplet size. For our samples, the advancing contact angles of the 1H, 1H-perfluorooctylamine-grafted or octadecylamine-grafted multifilament fabric surface become very close to 180° when the droplet begins to move. However, the receding contact angles are affected by the local structures of fabric such as protruding yarns, yarn size and yarn spacing on the surface. Although the receding contact angles are as small as 90°, the roll-off angles of these superhydrophobic surfaces were less than 5° when a 0.5 mL water droplet was applied.

DESIGN AND DEVELOPMENT OF

SUPERHYDROPHOBIC TEXTILE SURFACES

by

HOON JOO LEE

A dissertation submitted to the Graduate Faculty of
North Carolina State University
in partial fulfillment of the requirements for the degree of
Doctor of Philosophy

TEXTILE TECHNOLOGY MANAGEMENT

Raleigh, North Carolina

2007

APPROVED BY:

Dr. M. King	Dr. B. Pourdeyhimi
Dr. S. Michielsen Chair of Advisory Committee	Dr. T. J. Little Co-chair of Advisory Committee

BIOGRAPHY

Hoon Joo Lee received her Bachelor of Science degree in Textile Engineering in 1999 and obtained her Master of Science in Fiber and Polymer Engineering in 2003 from Hanyang University, Korea. In pursuit of further studies, she joined North Carolina State University to enroll her Doctoral program in Textile Technology Management in fall 2004. Upon completion of her Doctor of Philosophy degree, she plans to continue expanding her research interests in new product design and development for high tech textiles.

ACKNOWLEDGEMENTS

First and foremost, I would like to express my sincere gratitude and appreciation to my advisor Dr. Stephen Michielsen for giving me the opportunity to work for him, and for providing his continuous support throughout the entire study. This work would not have been possible without his wide experience and knowledge. I also appreciate the support, guidance, and encouragement given by Drs. Nancy Cassill and Trevor J. Little, my advisors in Textile Management. I wish to address a very special thanks to Drs. Martin King, Behnam Pourdeyhimi, Eunkyoung Shim and Tushar K. Ghosh for their kindness and guidance in finding my research direction. I also thank to Ms. Carolyn Krystoff and Mr. Robert W. Cooper for their kind help during my study.

Last but not the least, I would like to express my sincere appreciation, love, and gratitude to my mother who continues to love, encourage and support me through every adventure and challenge. My gratitude also extends to Drs. Subhash K. Batra, Moon W. Suh and Mrs. Chi S. Suh who have been such a big support and a source of encouragement during the entire study.

TABLE OF CONTENTS

LIST OF TABLES

LIST OF FIGURES

LIST OF SCHEMES

1. INTRODUCTION

A superhydrophobic surface is defined as having a water contact angle greater than 150° and a roll-off angle less than 5°.[1] [2] The high contact angle is obtained by a combination of surface chemistry and surface roughness while the roll-off angle depends on the droplet size and the contact angle hysteresis, which is the difference between the advancing and the receding contact angles.[3] A water droplet easily rolls off a superhydrophobic surface, washing dirt off in the process and effectively cleaning the surface. This unusual wetting behavior is called the Lotus effect or self-cleaning.[4] The Lotus effect is obtained by two criteria: a low surface energy and a well-designed surface roughness.[5] [6] [7] [8] [9] [10]

The amazing water-repellency, superhydrophobicity, of some plants has received a great deal of interest.[11] [12] There are two different types of water-repellent plant leaves: the first type is hair covered leaves such as Lady's Mantle, and the second type is macroscopically smooth leaves such as Lotus.[13] Water droplets completely run off both plant leaves and their surfaces remain dry even after heavy rain. Although this phenomenon is observed on other plants leaves besides the Lotus plant leaves, the ability has been termed the Lotus effect. For these surfaces, as water droplets roll off easily, they wash dirt off the leaves and effectively keep the surface clean.[14]

Technologies related to superhydrophobic treatments have recently attracted considerable attention due to their potential applications in medical devices as well as industrial materials. The idea of superhydrophobicity was introduced six decades ago by A. Cassie who, working for the British Council of the Wool Industries, was interested in enhanced water repellency.[15] This amazing water-repellency has been used in the textile industry ever since.

The objectives of this study are to compare the wetting behavior of a rough surface to that of a smooth surface; to analyze the relationship between the contact angle hysteresis and the sliding angles of water droplets; and to design and prepare superhydrophilic and superhydrophobic surfaces using textile structures. Since the wettability of a solid surface is determined by two parameters, the chemical composition and the geometrical structure of a rough surface, the combination of these two factors are used for the development of superhydrophobic surface.[16] On the other hand, in this study, a superhydrophobic rough surface is designed using a plain woven structure and prepared by grafting low surface tension materials such as 1H, 1H-perfluorooctylamine or octadecylamine to poly(acrylic acid) (PAA) grafted nylon 6,6 woven fabric consisting of multifilament yarns. The woven fabrics consist of conventional nylon fibers whose diameters are greater than 15 μm, which is much larger than the microfibers (diameter of < 5 μm) or nanometer sized structures used by other authors.[17] [18] [19] The wetting behavior of the superhydrophobic woven fabric is compared to that of other materials having a flat surface or a rough surface made of a woven fabric consisting of monofilament yarns.

2. LITERATURE REVIEW

2.1. Surface tension and contact angle

2.1.1. Contact angle and wettability

In general, contact angles are measured for the evaluation of the surface tension and wettability (Figure 2.1). [20] Although it is hard to measure the surface tension of a solid directly, it is easy to measure its contact angles. Therefore, the evaluation of surface tension through contact angle measurement has been studied by many researchers. The contact angles of polymers and organic layers can be used for the prediction of surface tension and wetting behavior for various liquids. [21] This can be explained as follows.

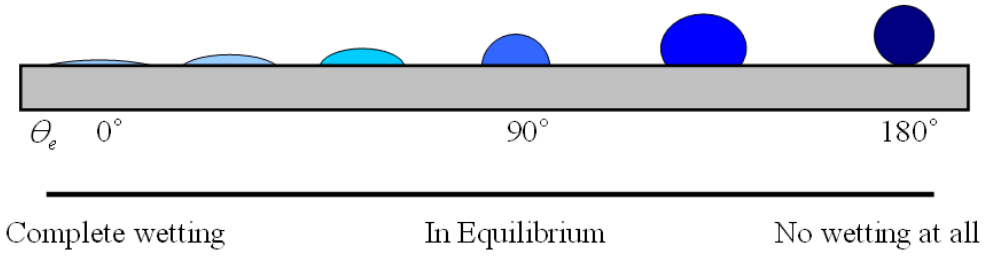

Figure 2.1. Contact angle and wettability.

The relation between the surface tension and contact angle is obtained by the Young equation:[22]

$$\frac{\gamma_{SV} - \gamma_{SL}}{\gamma_{LV}} = \cos\theta_e \qquad (2.1)$$

where γ is the surface tension; and SV, SL, and LV are the solid-vapor, the solid-liquid, and the liquid-vapor interfaces, respectively (Figure 2.2). According to Young's equation, the contact angle is a well-defined property that depends on the surface tension coefficients of solid, liquid and gas.

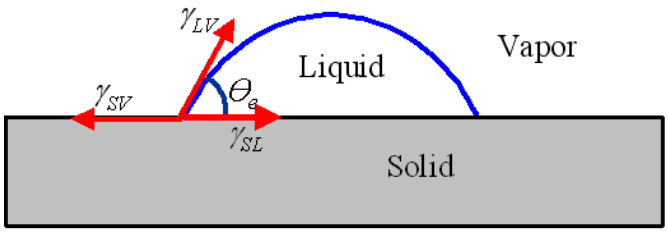

Figure 2.2. A drop on a flat surface.

The right hand side of equation (2.1) and γ_{LV} can be obtained from experimental measurements, leaving two unknowns, γ_{SV} and γ_{SL}. When θ_e for a test liquid > 20°, it is assumed that $\gamma_{SV} \approx \gamma_S$ and $\gamma_{LV} \approx \gamma_L$.[23] Equation (2.1) can then be reformulated as:

$$\frac{\gamma_S - \gamma_{SL}}{\gamma_L} = \cos\theta_e \tag{2.2}$$

Likewise, the thermodynamic work of adhesion can be explained by the Dupre equation as:

$$W_{SL}^a = \gamma_S^a + \gamma_L^a - \gamma_{SL}^a \tag{2.3}$$

Since the thermodynamic work of adhesion is the negative of the free energy of adhesion, the free energy of adhesion is also given by:

$$\Delta G_{SL}^{a} = \gamma_{SL}^{a} - \gamma_{S}^{a} - \gamma_{L}^{a}$$

Combining equation (2.2) and (2.3) results in the Dupre-Young equation:

$$W_{SL}^{a} = \gamma_{S}^{a} + \gamma_{L}^{a} - \gamma_{SL}^{a} = \gamma_{L}^{a}(1 + \cos\theta) \tag{2.4}$$

From equation (2.3), Lifshitz-van der Waals (*LW*) interaction energy between solid and liquid is:

$$W_{SL}^{LW} = (\gamma_{S}^{LW} - \gamma_{SL}^{LW}) + \gamma_{L}^{LW} = -\Delta G_{SL}^{LW} = \gamma_{L}^{LW}(1 + \cos\theta_{e}) \tag{2.5}$$

($\gamma_S - \gamma_{SL}$) from equation (2.5) can be obtained from contact angle measurements. Finally γ_S can be evaluated when γ_{SL} is known. The most frequently used method to assess γ_{SL} is the surface tension component approach, described in the next section.

2.1.2. Surface tension component approach

According to Fowkes, the interfacial tension between solid and liquid is given by the following equation when only dispersion interactions are present:[24]

$$\gamma_{SL}^{LW} = (\sqrt{\gamma_{S}^{LW}} - \sqrt{\gamma_{L}^{LW}})^{2} \tag{2.6}$$

The geometric mean of the liquid and solid surface tension is used to calculate the thermodynamic work of Lifshitz–van der Waals (*LW*) components:[25]

$$W_{SL}^{LW} = 2\sqrt{\gamma_{L}^{LW}\gamma_{S}^{LW}} \tag{2.7}$$

From equation (2.5), ${\gamma_{SL}}^{LW}$ is:

$${\gamma_{SL}}^{LW} = {\gamma_{L}}^{LW} + {\gamma_{S}}^{LW} - 2\sqrt{{\gamma_{L}}^{LW}{\gamma_{S}}^{LW}} = {\gamma_{L}}^{LW} + {\gamma_{S}}^{LW} + \Delta G_{SL}^{LW} \tag{2.8}$$

According to equation (2.8), γ_{SL}^{LW} increases as the free energy of solid-liquid interface increases.

Meanwhile, the addition of intermolecular forces at interfaces is equal to a surface tension of a material as shown in equation (2.9). [26] It is very important to understand the surface tensions on the right hand side of equation (2.8).

$$\gamma = \gamma^d + \gamma^p + \gamma^H + \gamma^{ind} + \gamma^m + ... \tag{2.9}$$

where *d*, *p*, *H*, *ind* and *m* mean London dispersion forces, permanent dipoles, hydrogen bonds, induced dipoles and metallic interaction, respectively. The solid or liquid surface tension can be obtained from equation (2.9) as:

$$\gamma_S = \gamma_S^d + \gamma_S^p + \gamma_S^H + \gamma_S^{ind} + \gamma_S^m ... \tag{2.10}$$

$$\gamma_L = \gamma_L^d + \gamma_L^p + \gamma_L^H + \gamma_L^{ind} + \gamma_L^m ... \tag{2.11}$$

Since the first three components in equation (2.10) and (2.11) are the major factors determining the surface tension of most of materials, we can use these group contribution methods to calculate γ_S and γ_L:

$$\gamma_S = \gamma_S^d + \gamma_S^p + \gamma_S^H \tag{2.12}$$

$$\gamma_L = \gamma_L^d + \gamma_L^p + \gamma_L^H \tag{2.13}$$

Combining equation (2.5), (2.7), (2.12) and (2.13) gives:

$$\gamma_L(1+\cos\theta) = \gamma_L^d(1+\cos\theta) + \gamma_L^p(1+\cos\theta) + \gamma_L^H(1+\cos\theta) = 2(\sqrt{\gamma_S^d \cdot \gamma_L^d} + \sqrt{\gamma_S^p \cdot \gamma_L^p} + \sqrt{\gamma_S^H \cdot \gamma_L^H}) \tag{2.14}$$

Since the surface tensions from London dispersion forces, permanent dipoles, and hydrogen bonds are:

$$\gamma_L^d(1+\cos\theta) = \gamma_S^d + \gamma_L^d - \gamma_{SL}^d = 2\sqrt{\gamma_S^d \gamma_L^d}$$

$$\gamma_L^p(1+\cos\theta) = \gamma_S^p + \gamma_L^p - \gamma_{SL}^p = 2\sqrt{\gamma_S^p \gamma_L^p}$$

$$\gamma_L^H(1+\cos\theta) = \gamma_S^H + \gamma_L^H - \gamma_{SL}^H = 2\sqrt{\gamma_S^H \gamma_L^H}$$

Table 2.1 shows surface tension of various materials.[20 21 23 26 27] Using this data, we can calculate liquid contact angles on polymer materials. For example, the water contact angle on Poly(tetrafluoroethylene, PTFE) is 117° according to equation (2.14), which is very close to the measured contact angle, 119°.

Table 2.1. Surface tension of various materials

Material	Surface tension (dyne/cm)			
	London dispersion forces	Permanent dipoles	Hydrogen-bonds	Total
Water	21.8	1.4	49.6	72.8
Decane	23.9	-	-	23.9
Dodecane	25.4	-	-	25.4
Hexadecane	27.6	-	-	27.6
Poly(ethylene)	31 ~ 31.5	-	-	31 ~ 31.5
Poly(propylene)	29.6	-	-	29.6
Poly(styrene)	30 ~ 36	-	-	30 ~ 36
Poly(hexafluoropropylene)	16.2 ~ 17.1	-	-	16.2 ~ 17.1
Poly(tetrafluoroethylene)	18.5	-	-	18.5
Nylon	40.8	-	6.2	47.0

The above approach works well when no strong attraction between the liquid and the surface exists. Lee added a contribution to the surface tension, γ^{AB}, to address this short coming. Thus, since the major additional interaction forces are from short-range chemical interactions at the interface, the surface tension can be described as:[28]

$$\gamma = \gamma^{LW} + \gamma^{AB} \tag{2.15}$$

where $\gamma^{LW} = \gamma^{d} + \gamma^{p} + \gamma^{ind}$ and AB means (Lewis) acid-base interactions.

2.2. Rough wetting

2.2.1. Wettability of rough surfaces

The Young equation is valid for only partial wetting of solid having a smooth surface, but real solids are not perfectly flat. The surface structure affects wettability.[29] [30] For example, liquid droplets are in contact with the upper part of a rough surface and the lower part is filled with air when the surface of solid is superhydrophobic.[31] [32] In this chapter, we study the apparent contact angle of a drop deposited on a textured surface, and finally characterize a hydrophobic surface.

Bico *et al.* pointed out a possible function of the roughness when a textured surface is in contact with liquid.[33] According to Bico, the interfacial energy will be changed as much as *dE* per unit area when the adsorption increases by a small quantity *dz*:

$$dE = (\gamma_{SL} - \gamma_S)(r - \Phi_S)dz + \gamma_L(1 - \Phi_S)dz \tag{2.16}$$

where r and Φ_S are the roughness of the textured solid and the area fraction of a solid surface in direct contact with the liquid. $\Phi_S = 1$ is the case of a fully wetted surface.

Figure 2.3 shows a micro-structured rough surface of a liquid reservoir. The total liquid quantity z decreases through adsorption when dE/dz is positive and increases when negative. Hence, the liquid will be in equilibrium when:

$$(\gamma_{SL} - \gamma_S)(r - \Phi_S) + \gamma_L(1 - \Phi_S) \approx 0 \tag{2.17}$$

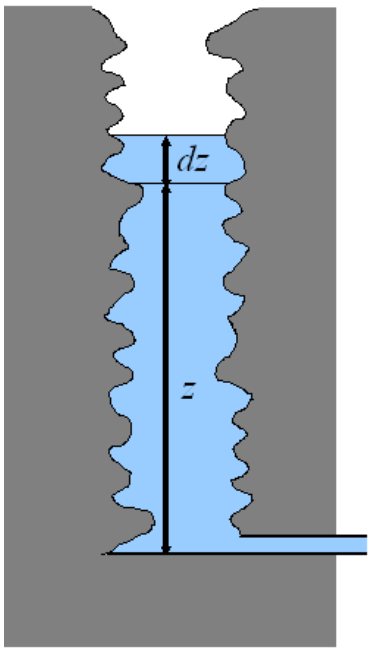

Figure 2.3. Rough surface of a liquid reservoir.

Using the Young equation, equation (2.17) can be reformed as:

$$\cos\theta_r = \frac{1-\Phi_S}{r-\Phi_S} \tag{2.18}$$

Equation (2.18) defines a critical contact angle between zero and $\pi/2$, since $r \geq 1$ and $\Phi_S \leq 1$. For example, the surface should be completely wet when r approaches one since the contact angle becomes zero, but the contact angle will be close to 90° when $r >> 1$ or $r > 1$ and $\Phi_S << 1$.

2.2.2. Hydrophobicity on rough surfaces

Roughness makes a significant contribution to the wetting behavior of a surface.[34] Since Young's equation is only appropriate for a flat surface, other expanded approaches are needed to describe the contact angle of a droplet on a rough surface.[35] [36] When the surface is roughened the minimization of liquid surface free energy results in two possible contact angles, the Wenzel apparent contact angle or the Cassie-Baxter apparent contact angle. [37] [38] Figure 2.4 shows the apparent contact angle on a rough surface.

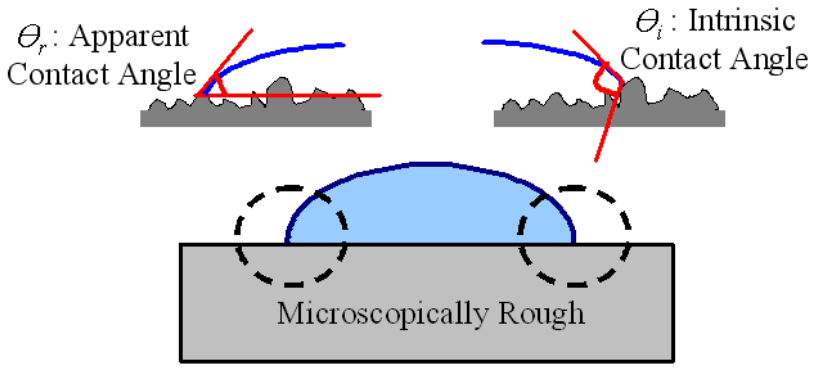

Figure 2.4. A drop on a rough surface.

In Wenzel's approach the liquid fills the grooves on the rough surface (Figure 2.5a). According to Wenzel, the liquid contact angle at a rough surface can be described as: [39]

$$\cos\theta_r^W = r\cos\theta_e \qquad (2.19)$$

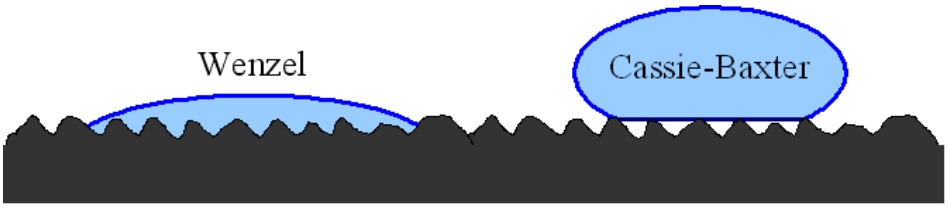

(a) (b)

Figure 2.5. A liquid drop (a) wetting the grooves of a rough surface (Wenzel model) and (b) sitting at the top of a rough surface (Cassie-Baxter model).

Here, r is the ratio of the total wet area of a rough surface to the apparent surface area in contact with the water droplet ($r > 1$). If the Young contact angle is smaller than a critical contact angle θ_c, the liquid is sucked into contact with the rough surface. According to equation (2.19), for large r, the rough surface is dry when the contact angle on a flat surface exceeds 90° (Figure 2.6).

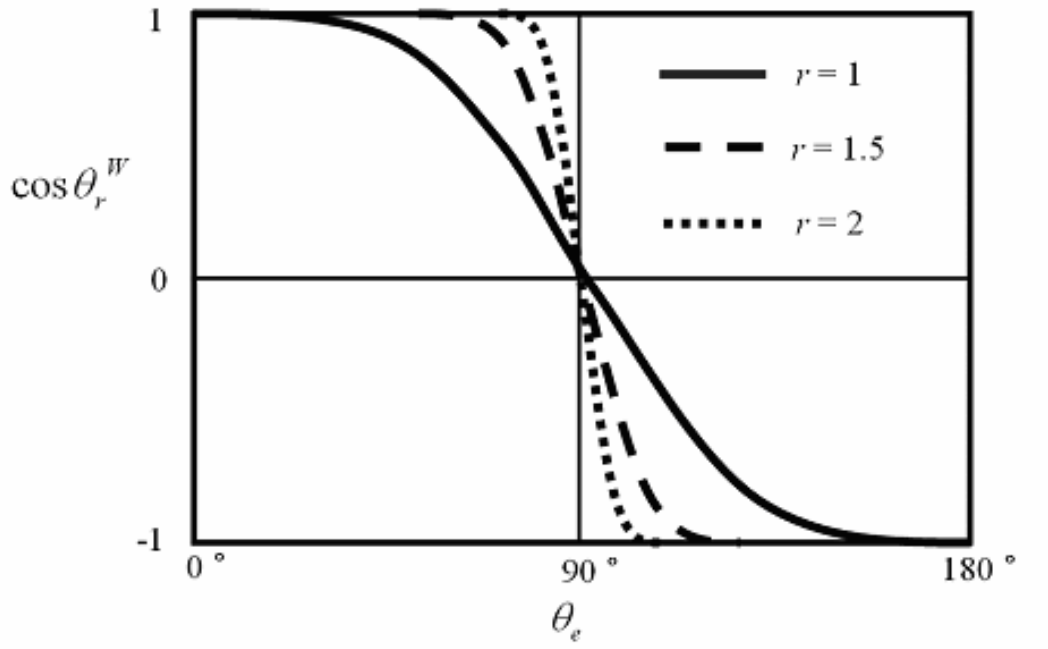

Figure 2.6. Cosine curves of apparent contact angles depending on roughness, *r*.

The Cassie and Baxter model is an extended form of the Wenzel model to include porous surfaces. In this model a liquid sits on a composite surface made of a solid and air. Therefore, the liquid does not fill the grooves of a rough solid. In their paper published in 1944, Cassie and Baxter suggested that:[40]

$$\cos\theta_r^{CB} = f_1 \cos\theta_e - f_2 \tag{2.20}$$

where f_1 is the surface area of the liquid in contact with the solid divided by the projected area, and f_2 is the surface area of the liquid in contact with air trapped in the pores of the rough surface divided by the projected area. According to Cassie and Baxter:

$$f_1 = \frac{\text{Area in contact with liquid}}{\text{Projected area}} \tag{2.21}$$

$$f_2 = \frac{\text{Area in contact with air}}{\text{Projected area}} \tag{2.22}$$

When there is no trapped air, f_1 is identical to the value of r in the Wenzel model. Recognizing this, equation (2.25) has recently been rewritten as follows:

$$f_1 = r_f f \tag{2.23}$$

$$f_2 = 1 - f \tag{2.24}$$

$$\cos\theta_r^{CB} = r_f f \cos\theta_e + f - 1 \tag{2.25}$$

where f is the fraction of the projected area of the solid surface in contact with the liquid and r_f is defined by analogy with the Wenzel model.[41] It is important to note that r_f in equation (2.25) is not the roughness ratio of the total surface, but only of that in contact with the liquid. In this form of the Cassie-Baxter equation, the contributions of surface roughness and of trapped air are much clearer than in the other forms of the equation.

Recently, many authors used another approach for the Cassie-Baxter equation to describe contact angles of droplets on heterogeneous rough surfaces that have composite interfaces.[42] In the modified Cassie and Baxter model the liquid forms a composite surface made of solid, liquid and air; and the liquid does not fill the grooves on the rough surface (Figure 2.5b).[43] When the top of a rough surface is completely flat, the following equation describes the apparent contact angle on a rough surface:[44]

$$\cos\theta_r^{CB} = \Phi_1 \cos\theta_1 + \Phi_2 \cos\theta_2 \tag{2.26}$$

where θ_r^{CB} is the apparent contact angle at a heterogeneous rough surface composed of two different materials; θ_1 and θ_2 are the droplet contact angles on the two surfaces. A unit area

of the surface has a unit surface area fraction Φ_1 with a contact angle θ_1 and an area fraction Φ_2 with a contact angle θ_2. When this rough surface consists of only two materials $\Phi_2 = 1 - \Phi_1$. If the liquid does not completely wet the surface, Φ_2 represents the trapped air with θ_2 =180º. Equation (2.20) can be modified as:[45]

$$\cos\theta_r^{CB} = \Phi_S \cos\theta_e + \Phi_S - 1 = \Phi_S(\cos\theta_e + 1) - 1 \tag{2.27}$$

$$\Phi_S = \frac{\Sigma a^2}{\Sigma(a+b)^2} \tag{2.28}$$

where Φ_S is the ratio of the rough surface area in contact with a liquid drop to the total surface covered by a liquid drop, a is the width of a prominence of a rough surface and b is the distance between prominences. Smaller Φ_S increases θ_r^{CB} and makes the surface more hydrophobic (Figure 2.7).

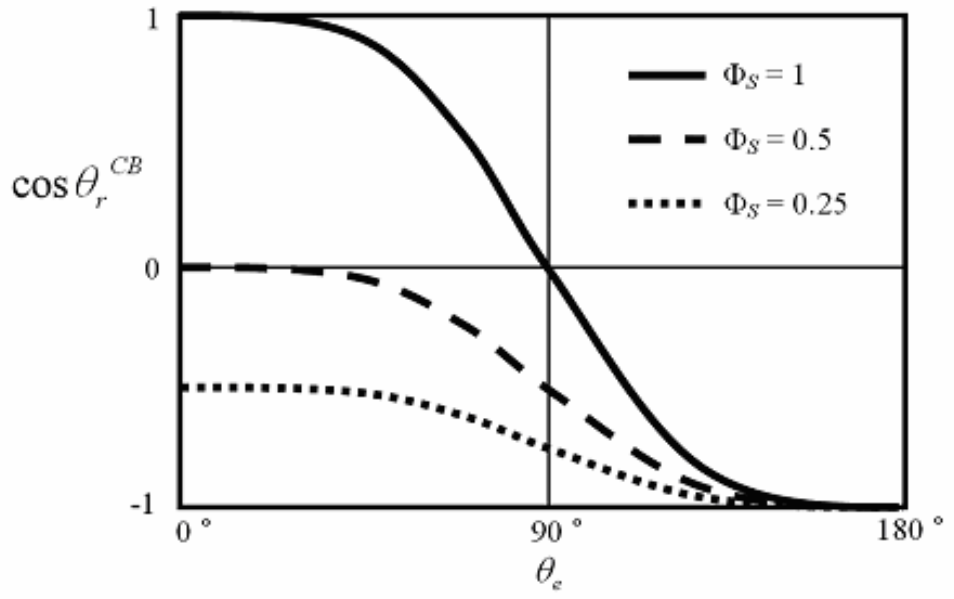

Figure 2.7. Cosine curves of apparent contact angles depending on top area fraction, Φ_S.

For an apparent contact angle of water on Teflon^{TM} to be greater than 150º (superhydrophobic), the fraction of the surface in contact with water must be less than 26%.[46]

2.2.3. Modeling of artificial lotus fabric

Although most studies of the Lotus effect have been carried out on inorganic materials, textile materials having a rough surface can also be superhydrophobic by the Lotus effect.[47] [48] In this case, the protruding fibers of woven or knitted fabric, flock fibers of flock fabric, or surface fibers of nonwoven fabric can be regarded as grooves of rough surfaces.[49] Figure 2.8 shows the upper-sectional view of a roughness pattern when the grooves are thought of as square pillars sticking up from a fabric substrate.[50] [51]

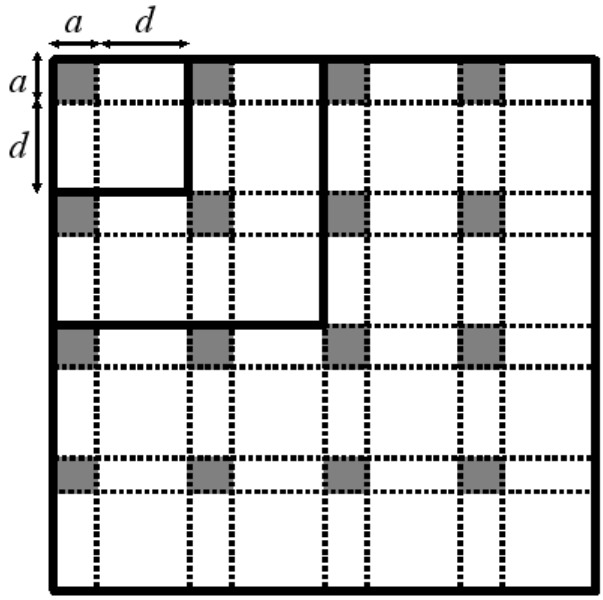

Figure 2.8. Upper-sectional view of roughness pattern.

The pillar cross-sectional area is a^2, the distance between two pillars is d, and the height of pillar is h. In an analysis of the superhydrophobic effect, Patankar has provided two equations to describe the surface based on the Wenzel (equation (2.19)) and the Cassie-Baxter (equation (2.21)) models:[52 53]

$$\cos\theta_r^W = \left(\left(\frac{a}{a+d}\right)^2 \frac{4h}{a} + 1\right)\cos\theta_e \tag{2.29}$$

$$\cos\theta_r^{CB} = \left(\frac{a}{a+d}\right)^2 (\cos\theta_e + 1) - 1 \tag{2.30}$$

As a numerical example, if a smooth surface is hydrophobic (θ_e = 120º), the width of a pillar is ten micrometers and the height of the pillar is one millimeter, the distance between two pillars, d, has to be 0.014 mm < d < 0.24 mm for a superhydrophobic surface.

In recent literature, the Cassie-Baxter model is often described using the apparent contact angle on a rough surface by equation (2.27).[54] [55] Note that the form of the Cassie-Baxter equation given in equation (2.27) is not generally valid. In fact, comparing equation (2.27) to equation (2.20) or equation (2.25), it is obvious that equation (2.27) is only valid when $r_f = 1$, i.e. when the liquid is in contact with a flat porous surface. The use of equation (2.27) should be restricted and the complete Cassie-Baxter equation in either the form given in equation (2.20) or the form given in equation (2.25) should be used.

2.3. Contact angle hysteresis

When the volume of a liquid drop placed on the surface by a syringe is steadily increased until the contact line advances, the contact line begins to move. The contact angle observed when it just begins to move is the advancing contact angle (θ_A). On the other hand, when the liquid droplet is retracted steadily until the contact line recedes, the contact line begins to move again. The contact angle observed when the contact line is just set in motion by this process is defined as the receding contact angle (θ_R).[56] Alternatively if the surface with a drop on it is slightly tilted, the drop remains with different contact angles at the front and the back of the drop. Barthlott and Neihuis suggested that the advancing contact angle of a water droplet easily reaches the receding contact angle on a self-cleaning rough surface when the surface is slightly tilted. Thus, the drop easily rolls off of this surface, washing dirt off and cleaning the surface in the process as shown in right side of Figure 2.9.[57] Their analysis differs from recent literature. Dorrer and Ruehe proved that the advancing contact angle on a superhydrophobic surface is not affected by the surface roughness and reaches to 180° during the advancing motion; in contrast, the receding contact angle is strongly influenced by several geometric parameters such as the shape, size and spacing of the protuberances of the surface.[58] Yoshimitsu *et al.* showed that the roll-off angles are in inverse proportion to the weight of a water droplet and the proper design of a rough surface is more important than increasing roughness to obtain a better sliding behavior.[59] According to Brandon *et al.*, the contact angle hysteresis decreases as the

volume of the drop increases.[60] In addition, Hennig *et al.* demonstrated that the contact angle hysteresis of a smooth film depends on the contact time with water.[61]

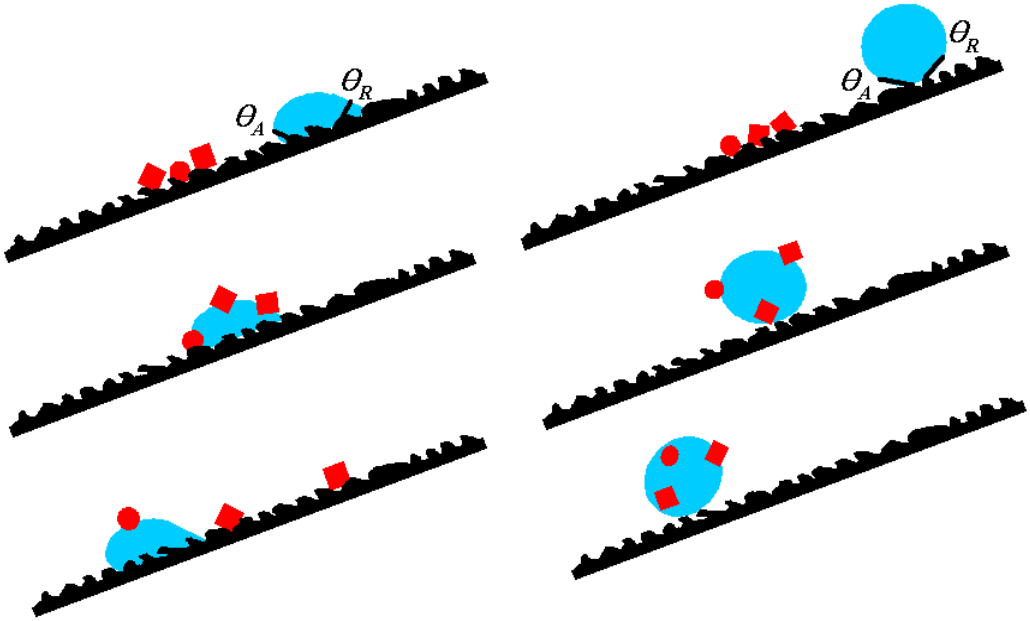

Figure 2.9. Self-cleaning effect by superhydrophobicity.

Since surface debris sticks to the drop surface and is removed when the drop rolls off, the superhydrophobic surface has self-cleaning effect. The difference between the advancing angle and the receding angle is the contact angle hysteresis defined as $\Delta\theta_H$. The contact angle hysteresis is very important in understanding the drop motion on a surface.

2.3.1. Sliding angle

The sliding angle of droplets on smooth surface can be described as:[62]

$$mg\sin\alpha = k2\pi R \tag{2.31}$$

where α is the sliding angle, R is the radius of the contact circle, m is the mass of the droplet, g is the gravitational acceleration, and k is a proportionality constant. Roura and Fort demonstrated the work due to the external forces on a drop in Figure 2.10.[63]

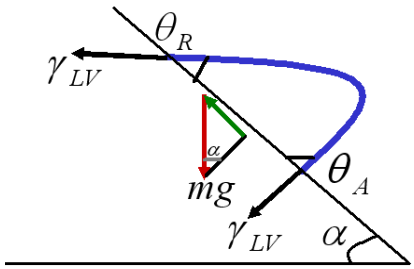

Figure 2.10. Water drops on a tilted surface.

Figure 2.10 shows that the advancing contact angle is always greater than the receding contact angle on a tilted surface. This condition was described by Furmidge as:

$$mg\sin\alpha \approx -2R\gamma_{LV}(\cos\theta_A - \cos\theta_R) \tag{2.32}$$

When the surface is tilted, the tilt angle increases until the drop begins to move and equation (2.32) can be expressed in terms of working energy if the drop slides down as shown in Figure 2.10.

As mentioned before, it is assumed that the receding contact angle and the advancing contact angle seem to be close to their minimum and maximum values, respectively when the drop slides down ($\alpha = \alpha_c$):

$$mg\sin\alpha_c \approx -2R\gamma_{LV}(\cos\theta_{A(\max)} - \cos\theta_{R(\min)}) \tag{2.33}$$

Equation (2.33) shows an energy balance when the solid surface is progressively inclined and the drop begins to slide at α_c. In this situation, gravity can supply the necessary energy to develop the back wetted surface, and thereby the energy used to create a unit area of this surface is $-2R\gamma_{LV}(\cos\theta_{A(\max)} - \cos\theta_{R(\min)})$. Although the contact angle changes continuously along the contact line, equation (2.33) can be approximately calculated. The constant k in equation (2.31) is related to contact angle hysteresis, and the interfacial surface tension between water and vapor.

When the surface is superhydrophobic and the droplet is close to spherical:

$$m = \frac{4}{3}\pi(R')^3\rho \tag{2.34}$$

where ρ is the density of water and R' is the radius of droplet. By multiplying $g\sin\alpha_c$ to both sides we can describe the relationship between the radius of the contact circle and the radius of droplet sliding on a smooth surface as:

$$mg\sin\alpha_c = \frac{4}{3}\pi(R')^3\rho g\sin\alpha_c \tag{2.35}$$

Substituting equation (2.35) into equation (2.33), we obtain:

$$\sin\alpha_c = k'(\cos\theta_{A(\max)} - \cos\theta_{R(\min)}) \tag{2.36}$$

where k' is constant. Referring to equation (2.33), k' is related to the radius of the contact circle, the interfacial surface tension between water and vapor, and the contact angle hysteresis.

2.3.2. Contact angle hysteresis

The concept of gain factors is visualized in Figure 2.11 by numerical computations. The gain factor is considered as the rate of variation of the contact angle hysteresis at any operating point.[64] The Wenzel gain factor graph shows gain factors equal to the roughness factors for the region close to $\theta_e = 90°$, and the gain factors dramatically increase on either side of this region. The Cassie-Baxter gain factors increase from zero to maximum value of one.

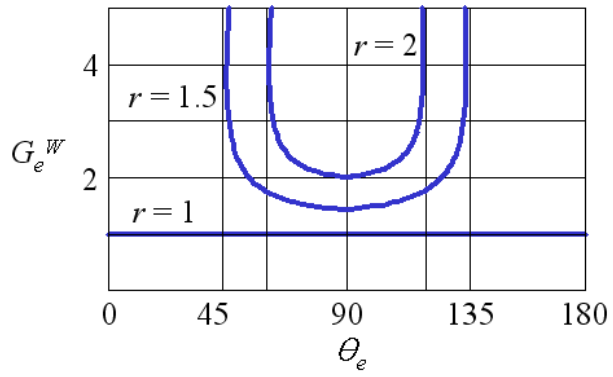

(a)

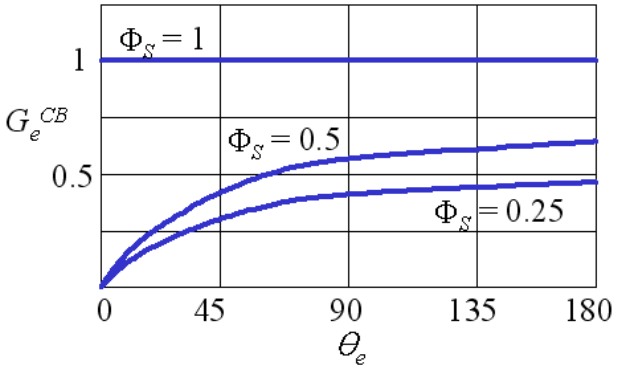

(b)

Figure 2.11. Gain factors on rough surfaces for (a) r = 1, 1.5 and 2 (Wenzel model) and (b) Φ_S = 0.25, 0.5 and 1 (Cassie-Baxter model).

The Wenzel equation gives a change in the Wenzel contact angle, $\Delta\theta_H^W$, caused by a change in the contact angle on the smooth surface, $\Delta\theta_H$, as:

$$\Delta\theta_H^W = r\left(\frac{\sin\theta_e}{\sin\theta_r^W}\right)\Delta\theta_H = G_e^W\Delta\theta_H \tag{2.37}$$

where G_e^W is the Wenzel gain factor, and is $\partial\theta_r^W / \partial\theta_e$. The gain factor is very useful, for it separates the idea of the equilibrium contact angle increase occurring by surface

topography from the observed contact angle. Using the Wenzel equation we can obtain the Wenzel gain factor as follows:

$$\cos^2\theta_r^W = r^2\cos^2\theta_e$$

$$1-\cos^2\theta_r^W = 1-r^2\cos^2\theta_e$$

$$\sin\theta_r^W = \sqrt{1-r^2\cos^2\theta_e}$$

$$G_e^W = \frac{r\sin\theta_e}{\sin\theta_r^W} = \frac{r\sin\theta_e}{\sqrt{1-r^2\cos^2\theta_e}} \tag{2.38}$$

When a contact angle θ_e is close to 90° the Wenzel gain factor is approximately unity. Since the effect of roughness is proportional to the radian contact angle changes, the Wenzel gain factor rapidly increases as the roughness factor increases.

Likewise, Cassie-Baxter equation gives a change in the Cassie-Baxter contact angle, $\Delta\theta_H^{CB}$, caused by a change in the contact angle on the smooth surface, $\Delta\theta_H$, as:

$$\Delta\theta_H^{CB} = \Phi_S\left(\frac{\sin\theta_e}{\sin\theta_r^{CB}}\right)\Delta\theta_H = G_e^{CB}\Delta\theta_H \tag{2.39}$$

In a similar manner as above, a Cassie-Baxter gain factor, G_e^{CB}, can be obtained by the Cassie-Baxter equation as follows:

$$\cos^2\theta_r^{CB} = \left[\Phi_S(\cos\theta_e+1)-1\right]^2$$

$$1-\cos^2\theta_r^{CB} = 1-\left[\Phi_S(\cos\theta_e+1)-1\right]^2$$

$$\sin\theta_r^{CB} = \sqrt{1-\left[\Phi_S(\cos\theta_e+1)-1\right]^2}$$

$$G_e^{CB} = \frac{\Phi_S \sin\theta_e}{\sin\theta_r^{CB}} = \frac{\Phi_S \sin\theta_e}{\sqrt{1-\left[\Phi_S(\cos\theta_e + 1) - 1\right]^2}} \tag{2.40}$$

Since $\Phi_S \leq 1$, $G_e^{CB} \leq 1$. The θ_e used in equations (2.37) and (2.39) can be either the advancing or receding contact angles. Thus, the contact angle hystereses are:

$$\Delta\theta_H^W = G_e^W \Delta\theta_H$$

$$\Delta\theta_H^{CB} = G_e^{CB} \Delta\theta_H$$

According to McHale, the gain factor, G_e^{CB}, is an attenuation of any contact angle hysteresis, while hysteresis increases on a Wenzel-type surface. As a numerical example, if the average contact angle on the smooth surface is 70° and the contact-angle hysteresis is 50°, then a roughness factor of 1.9 gives a Wenzel contact angle of 50° and a gain factor of 4.3 so that the hysteresis on the rough surface will be increased to 172°. However, when θ_e is 120° and Φ_S = 1% after roughening, a Cassie-Baxter surface gives an apparent contact angle of 162° and a gain factor of 0.03, reducing the contact-angle hysteresis on the rough surface to 9.5°.

3. PRODUCT AND TECHNOLOGY REVIEW

3.1. Research review

Over the last 15 years, many studies of superhydrophobicity and contact angle hysteresis have been performed. Recently, Zhu *et al.* developed a superhydrophobic surface by electrospinning using a hydrophilic material, poly(hydroxybutyrate-co-hydroxyvalerate) (PHBV). [65] Gao and McCarthy made artificial super-hydrophobic surfaces with conventional polyester and microfiber polyester fabrics rendered hydrophobic by using a simple patented water-repellent silicone coating procedure. [66] Lee and Michielsen developed superhydrophobic surfaces via the flocking process and achieved contact angles as high as 178°. [67] Jopp *et al.* researched the wetting behavior of water droplets on periodically structured hydrophobic surfaces and the effect of structure geometry.[68] Liu *et al.* studied the creation of stable superhydrophobic surfaces using vertically aligned carbon nanotubes.[69] Nakajima *et al.* prepared superhydrophobic thin films with TiO_2 photocatalyst by coating a fluoroalkyl silane onto the original films.[70] Zhai *et al.* demonstrated that the superhydrophobic behavior of the lotus leaf structure can be achieved by creating a semifluorinated silane coated polyelectrolyte multilayer surface.[71] Han et al. created a superhydrophobic surface using a block copolymer micelle solution and silica nanoparticles. He also provided a strategy for the fabrication of a wettability-controlled organic-inorganic hybrid. Many other studies of superhydrophobicity have been accomplished in inorganic materials.[72] Huang *et al.* showed a superhydrophobic surface from nanostructure materials

can be applied to microfluidic devices by preparing a stable superhydrophobic surface via aligned carbon nanotubes (CNTs) coated with a zinc oxide (ZnO) thin film.[73] Shang *et al.* prepared optically transparent superhydrophobic silica-based films on glass substrates by making a nanoscale rough surface using nanoclusters and nanoparticles.[74] Shi *et al.* obtained a superhydrophobic surface by modifying a silver covered silicon wafer with a self-assembled monolyer of n-dodecanethiol.[75] Although most studies of the Lotus effect have been carried out on inorganic materials, organic composite materials having a rough surface can also be superhydrophobic by the Lotus effect. Jeong *et al.* fabricated micro/nanoscale hierarchical structures using a molding technique.[76] To modify an organic film surface and create superhydrophobicity, Kim *et al.* used He plasma and CF_x nanoparticle coatings and Fresnais *et al.* applied CF_4 and O_2 plasma.[77] [78]

3.2. Patent review

Baumann *et al.* invented a process for self-cleaning surface production.[79] They used glass, ceramic, plastic and metal as substrates and glazed substrates with superficially hydrophobic structured coating and physically changed the surface structure. They used very small particles with an average diameter of less than 100 nm, in particular 5 to less than 50 nm, for formation of the structure of the coating. Baumann *et al.* says "compositions according to the invention which are employed for the production of the structured coating of substrates according to the invention comprise, in addition to the structure-forming particles, a layer-forming material in a weight ratio of 100:1 to 1:2, in particular 20:1 to 1:1." The coating was distinguished by its transparency in order to make good self-cleaning properties. That means the use of the invention is for making superhydrophobic (self-cleaning) glass articles. Baumann *et al.* developed this technology and applied another patent in 2005.[80] This time they used coating layer containing a glass flux and structure-forming particles with a mean particle diameter within the 0.1 to 50 nm range. According to them, the glass flux and structure-forming particles are present in a volume ratio within the 0.1 to 5 range, and the micro-rough surface structure has a ratio of mean profile height to mean distance between adjacent profile tips within the 0.3 to 10 range. The substrate was coated with a composition containing a glass flux and structure-forming particles, and the layer was burnt to be superhydrophobic. Finally, the substrate obtained self-cleaning effect.

Buchsel *et al.* invented method of producing self-cleaning and non-adhesive paper or paper-like material.[81] The patent describes that a micro-structured paper or paper-like material having a self-cleaning and/or non-adhesive effect is hydrophobic across the entire cross-section of the material. The surface of materials is micro-structured in such a way that the surface is provided roughness whereby the distance between the elevations ranges from 0.04 to 100 μm and the height of the elevations ranges from 0.04 to 100 μm. This material contains particles having the size of 0.04 to 50 μm that are bound to the paper or paper-like material through binding. The paper or paper-like material becomes hydrophobic across the entire cross section of the material and has self-cleaning effect.

Kaibel *et al.* developed micro-structured, self-cleaning catalytically active surface.[82] The invention provides a microstructured, self-cleaning surface, with changing surface structures and comprising a catalytically active material in the depressions. The invention also provides a process of production of a microstructured, self-cleaning, catalytically active surface and a catalyst molding. In molding system, a support surface is powder coated with particles having a size of from 0.05 to 200μm and coated with a catalytically active material. According to Kaibel *et al.*, in a preferred embodiment of the process, i) a base layer of metal is applied to a support surface by layer deposition from solution if desired, ii) a first layer of metal containing embedded particles with a size of from 0.05 to 200μm is applied by layer deposition from a solution containing these particles in dispersed form on the support surface or the surface of the base layer, and iii) the first layer is coated

with a catalytically active second layer. Then, the substrate has microstructured crystal coating for self-cleaning effect.

Nun and Oles invented a self-cleaning surface that has antimicrobial properties.[83] Their invention is a process for the production of an antimicrobial self-cleaning surface. One or more antimicrobial polymer(s) is used for a surface-coating system for securing structure-formers to generate a self-cleaning surface. This method lastingly binds antimicrobial polymers to the self-cleaning surface. In 2005, Nun *et al.*, invented a shaping method for producing shaped bodies with at least one surface having self-cleaning properties, and also made shaped bodies produced according to this method.[84] The invention relates to shaping processes for producing moldings. That shaping body has at least one self-cleaning surface formed by microparticles and thermal shaping (molding) of materials comprising organic compounds. According to the patent, the process of the invention generates surfaces with self-cleaning properties prior to the thermal shaping, applying microparticles to the inner surfaces of the mold and then carrying out the molding process. In molding process, the microparticles are pressed into the surface of the molding before solidifying the surface. The patent also says "the process of the invention may be used in thermal shaping processes selected from blow molding, extrusion blow molding, extrusion stretch blow molding, injection blow molding, injection stretch blow molding, thermoforming, vacuum stretch forming, pressure stretch forming, and rotary thermoforming." The process seems to be good for producing three-dimensional articles, such as bottles, bumpers, drums, and so on. The process is simple since it uses existing

equipment. At least one surface from this molding has self-cleaning effect and the surface has particles with a fissured structure.

Wang also invented the Lotus leaf-like self-cleaning surface structure.[85] A self-cleaning surface structure formed of a coating mixture covered on the surface of a product. The coating mixture contains a polymeric resin having low surface tension and a nano sized metal oxide compound (i.e., nanosize TiO_2). The polymeric resin serves as a medium to bond the nano sized metal oxide to the surface of the product.

3.3. Applications in industry

BASF researchers developed the Mincor™ coating system in which they applied the Lotus effect observed in nature.[86] The effect of their laboratory product is based on a combination of nanoparticles and hydrophobic polymers.[87] Mincor™ is applicable not only to textiles but also to mineral plasters, concrete, brick facing, and even to wood (Figure 3.1).[88]

(a) (b)

Figure 3.1. A water droplet (a) on a wood surface coated with Mincor™ and (b) containing dirt on a superhydrophobic surface. (Source: BASF Photos).

Thus, Mincor™ can be used as an adhesive to improve hydrophobic effect in the area of construction. The extreme water repellency of this spray minimizes the adhesion among water drops and material surfaces; rain water rolls off immediately; and the surface is always dry and clean.

A textile company in Burlington, NC, also used the secret of the Lotus leaves for their research. Several years ago, scientists in Nano-Tex™ tried to make fabric repel water

without affecting the appearance, hand and breathability of the material.[89] The principle of their product is from billions of microsize protrusions dotting the waxy surface of the Lotus leaves. These protrusions of the Lotus leaves reduce the contact area between pollutant and the surface of the leaves, and thereby prevent anything sticking to its surface. To mimic this effect in the lab, Nano-Tex™ scientists mixed a colorless liquid polymer with 0.1μm sized silver particles; applied these chemicals to textile fabric; and heated it.[90] The particles were bonded to the surface of the fibers by heating and created a shield that prevents contaminant sticking. Unlike treatment using spray, Nano-Tex™ built superhydrophobicity right on the fibers within the fabric.[91] When they applied their chemicals to a cotton swatch for a test the mixture was bonded to the fabric forming an invisible coating, and the material obtained water repellency.

4. EXPERIMENTAL

4.1. Materials

Nylon 6,6 film (M_n:12 kD), nylon 6,6 multifilament plain woven fabric (weight: 100 g/m^2), nylon 6,6 monofilament plain woven fabric (weight: 100 g/m^2), nylon 6,6 calendered monofilament modified twill woven fabric (weight: 100 g/m^2), and flock fabrics were used as smooth or rough surfaces. To prepare flock fabrics, various nylon 6,6 rod-shaped short fibers (flock, Cellusuede), polyester fabric (93 g/m^2), acrylic adhesive (C. L. Hauthaway & Sons Co.), and an electrostatic flock applicator (CP-70, Cellusuede Products. Inc.) were used. Poly(acrylic acid) (PAA, M_w: 450 kD, Aldrich), 4-(4,6-dimethoxy-1,3,5-triazin-2yl)-4-methylmorpholinium chloride (DMTMM, Fluka), sodium thiocyanate (NaSCN, Fisher), methanol (CH_3OH, Aldrich), 1H, 1H-perfluorooctylamine ($C_8H_4F_{15}N$, Synquest), and octadecylamine ($C_{18}H_{39}N$, Aldrich) were used without further purification.

4.2. Preparation of rough nylon surfaces

The electrostatic flock applicator produces a 30 to 70 kV potential to drive the rod-shaped nylon flocks from the container of applicator to the polyester substrate fabric resting on a metal grounding plate (Figure 4.1). A 10x10 cm^2 polyester fabric was coated with 0.3 g of acrylic adhesive by screen-printing. The nylon flock was shot from the applicator for five seconds vertically down into the adhesive that had previously been applied to a polyester substrate. The flock fibers oriented in the flow direction to reduce their air resistance through this process, and those fibers were perpendicularly aligned to the polyester substrate. The fabric was dried at 120 for 10 minutes and cured at 149 °C for 5 minutes after pre-cleaning to remove unattached flock.

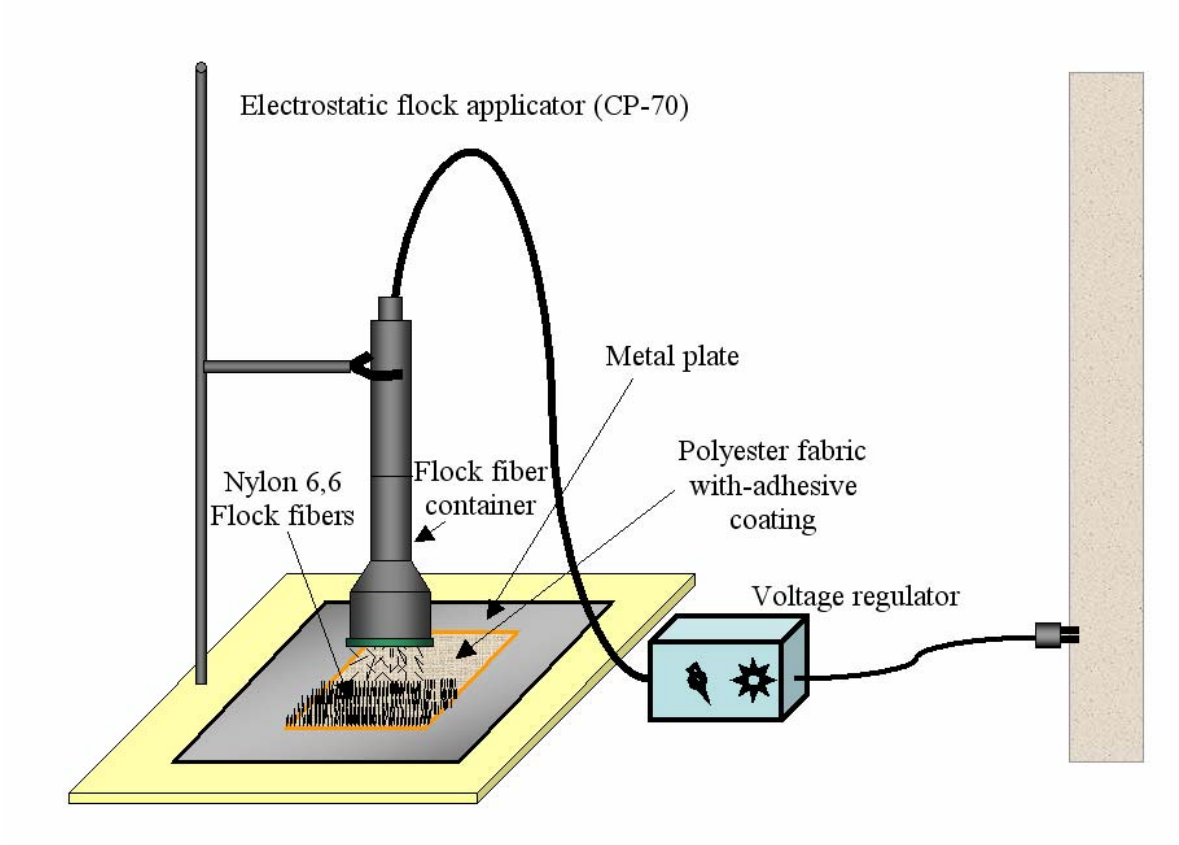

Figure 4.1. Application of nylon short fibers to polyester substrate using CP-70.

4.3. Surface modification of nylon 6,6

4.3.1. Grafting of PAA on nylon 6,6 surface

Since nylon 6,6 has few reactive groups on the surface and since we wish to chemically graft an alkyl or fluoroalkyl material to the surface, poly(acrylic acid), PAA, was first grafted to the nylon surface to increase the number of reactive sites following the procedure developed by Thompson.[92] 1 g PAA was dissolved in 250 mL distilled water at 20 ºC. Then 0.5 g nylon film (10 x 10 cm^2) and 1g of each nylon woven fabric (10 x 10 cm^2) were immersed in the PAA solution for 24 hours, rinsed in distilled water with stirring for 8 hours (repeated three times with fresh water), wiped with Kimwipes® and air dried.

0.1 g DMTMM was dissolved in distilled water with vigorous stirring at 20 ºC. PAA adsorbed nylon materials were immersed in the DMTMM solution to graft PAA to the nylon surfaces. The reaction was allowed to proceed for 2 hours. PAA-grafted nylon materials were rinsed in distilled water for 8 hours (repeated three times with fresh solvent), wiped with Kimwipes®, and air dried.

To remove non-grafted PAA, the nylon materials were rinsed in a 1 M aqueous sodium thiocyanate (NaSCN) solution with stirring (repeated twice with fresh solution), rinsed in distilled water for 8 hours (repeated three times with fresh solution), and heated in water for 3 hours at 65 ºC. Then, the nylon surfaces were wiped with Kimwipes® and air dried. Scheme 4.1 shows the grafting procedure of PAA on nylon 6,6.

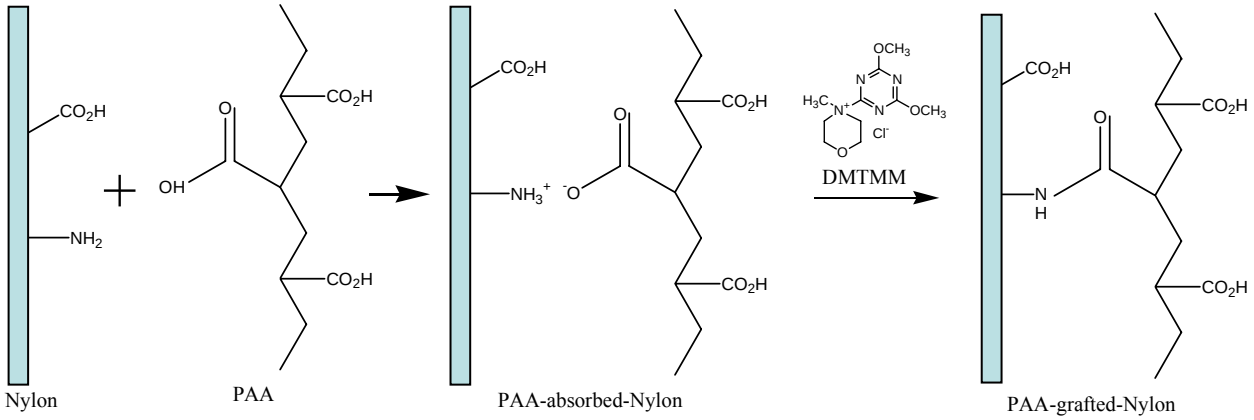

Scheme 4.1. Graft of PAA on nylon 6,6.

4.3.2. Grafting of fluoroamine on PAA-grafted nylon 6,6 surface

0.05 g 1H, 1H-perfluorooctylamine was dissolved in 10 mL methanol at 20ºC. Then 0.15 g PAA-grafted nylon film (5 x 6 cm^2) and 0.3 g of each PAA grafted nylon woven fabric (5 x 6 cm^2) were immersed in the 1H, 1H-perfluorooctylamine solution for 24 hours with stirring to allow adsorption of 1H, 1H-perfluorooctylamine.

0.03 g DMTMM was dissolved in methanol with vigorous stirring at 20ºC. 1H, 1H-perfluorooctylamine adsorbed PAA-grafted nylon materials were immersed in the DMTMM solution to graft 1H, 1H-perfluorooctylamine to the PAA on nylon 6,6 surfaces. The reaction proceeded for 2 hours. The 1H, 1H-perfluorooctylamine-grafted PAA-grafted nylon materials were rinsed in methanol for 8 hours (repeated twice with fresh solvent), rinsed in distilled water for 8 hours (repeated twice with fresh solvent), wiped with

Kimwipes®, and air dried. Scheme 4.2 shows the grafting procedure for 1H, 1H-perfluorooctylamine on PAA-grafted nylon 6,6.

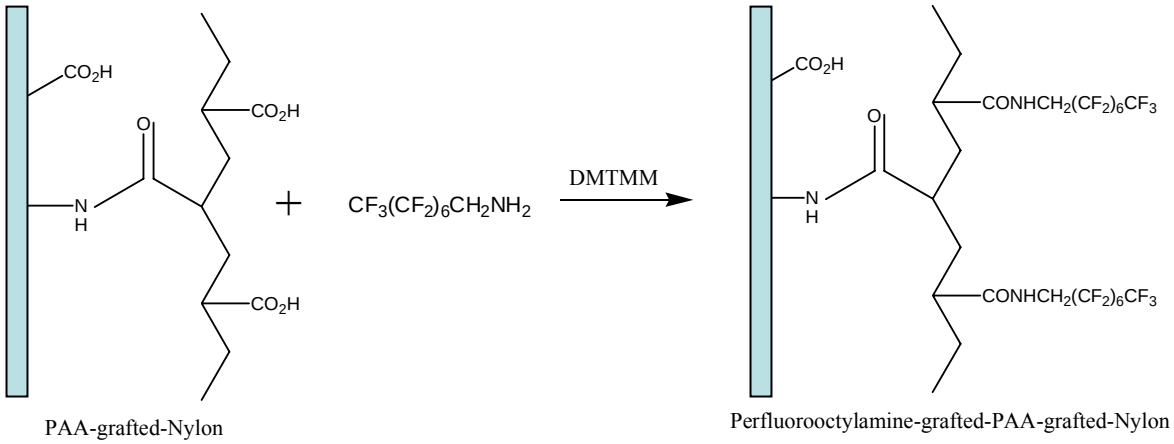

Scheme 4.2. Graft of 1H, 1H-perfluorooctylamine on PAA-grafted nylon 6,6.

4.3.3. Grafting of octadecylamine on PAA-grafted nylon 6,6 surface

0.03 g octadecylamine was dissolved in 10 mL methanol at 20ºC. Then 0.15 g PAA-grafted nylon film and 0.3 g of each PAA-grafted nylon woven fabric were immersed in the octadecylamine solution for 24 hours with stirring to allow adsorption of octadecylamine.

0.03 g DMTMM was dissolved in methanol with vigorous stirring at 20 ºC. Octadecylamine adsorbed PAA-grafted nylon materials were immersed in the DMTMM solution to the graft octadecylamine to the PAA on nylon 6,6 surfaces. The reaction proceeded for 2 hours. The octadecylamine-grafted PAA-grafted nylon materials were rinsed in methanol for 8 hours (repeated twice with fresh solvent), rinsed in distilled water

for 8 hours (repeated twice with fresh solvent), wiped with Kimwipes®, and air dried. Scheme 4.3 shows the grafting procedure for octadecylamine on PAA-grafted nylon 6,6.

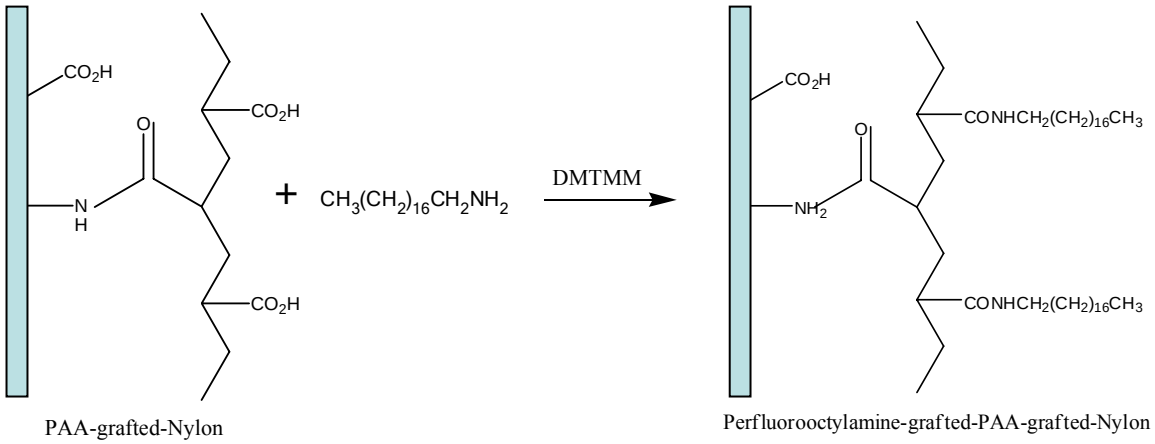

PAA-grafted-Nylon

Perfluorooctylamine-grafted-PAA-grafted-Nylon

Scheme 4.3. Graft of octadecylamine on PAA-grafted nylon 6,6.

4.4. Characterization

4.4.1. Scanning electron microscopy

The rough surface nylon composite was examined with a scanning electron microscope (SEM), Hitachi S-3200N, operated at 5 kV and 10 kV and magnifications from 25x to 2000x magnification. Image J 1.34s (National Institute of Health) was used for image analysis of SEM pictures. On a rough surface, the diameters and distances among adjacent protuberances or grooves were measured using this program.

4.4.2. Contact angle measurements

The contact angle on the prepared surfaces was measured from sessile water drops using a lab-designed goniometer at 20 . The contact angle images were obtained using an optical contact angle instrument (VCA Optima, AST Products Inc.) and a high resolution zoom camera (Century Optics .65X or VPLL-ZM101, Sony Corp.). The volumes of the applied droplets of distilled water were 10, 20 and 50 μL. Mean values were calculated from at least four individual measurements each on a new spot. The roll-off angle was measured by placing a specimen on a level platform mounted on a rotation stage, Newport 495, and inclining the specimen. 10, 20, 50, and 500 μL of water droplets were placed onto the surface, and the angle of the stage was recorded when the drop rolled off.

5. RESULTS AND DISCUSSIONS

To form a superhydrophobic surface, the surface must have a low surface tension and be rough. We used a two stage procedure to create a superhydrophobic fabric. First, we modified nylon film to generate a low surface tension surface. Then we made a rough nylon surface via the flocking process and modified the nylon flock fibers to give them a low surface tension using the same procedure as for the nylon film. Similar studies were performed on woven fabrics and calendered woven fabrics. A water droplet easily rolled off of the superhydrophobic surfaces at a very low incline angle.

5.1. Chemical surface modification of nylon 6,6

The wetting behavior of a solid surface is controlled by both the surface tension and the geometric structure of the surface. To form a superhydrophobic surface, the surface has to have a low surface tension and an appropriate roughness. First, we verified that the chemical procedure described in the experimental section resulted in a low surface energy on smooth nylon 6,6 films.

According to Equation (2.14), a water droplet (γ_L^d = 21.8, γ_L^p = 1.4, and γ_L^H = 49.6 dyne/cm) placed upon a clean, smooth nylon surface (γ_S^d = 40.8 and γ_S^H = 6.2 dyne/cm) should have a contact angle θ_e = 72º.[20 21 23 26 27] The values of the water contact angles measured on clean nylon film in this study are 65º ≤ θ_e ≤ 73º, in good agreement with the

predicted value as shown in Table 5.1. Figure 5.1 presents a water droplet sitting on a smooth nylon film; the equilibrium water contact angle on this surface is 70º.

Table 5.1. Comparison of predicted and measured water contact angles on smooth surfaces

Sample	Contact Angle (degree)	
	Predicted	Measured
Nylon	$\theta_e = 72$	$65 \leq \theta_e \leq 73$
PAA-grafted nylon	$\theta_e < 65$	$43 \leq \theta_e \leq 50$
1H, 1H-perfluorooctylamine-grafted PAA-grafted nylon	$\theta_e > 73$	$93 \leq \theta_e \leq 110$
Octadecylamine-grafted PAA-grafted nylon	$\theta_e > 73$	$95 \leq \theta_e \leq 102$

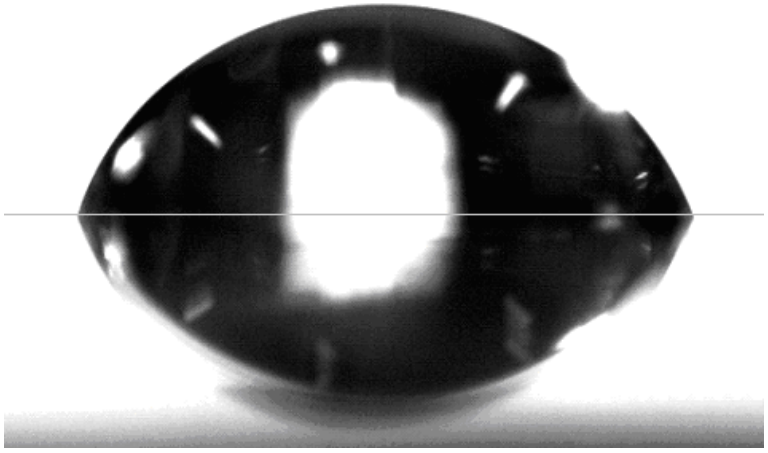

Figure 5.1. A water droplet on a smooth nylon surface. The water contact angle on this surface is 70º. Thin gray line indicates the film surface.

To make the nylon film surface hydrophobic, we need to attach a low surface tension material to the nylon surface. However, nylon has very few reactive sites, so first we must modify the surface to increase the number of reactive sites. Using the procedure developed by Tobiesen and Michielsen[93] and as modified by Thompson,[92] we first grafted PAA onto the film. Using multiangle x-ray photoelectron spectroscopy, XPS, Thompson found that the PAA layer on nylon 6,6 was approximately 10nm thick.[92] PAA was used as a mediator between nylon 6,6 and a fluoroamine due to the high density of carboxylic acid groups along the backbone of PAA. The carboxylic acid groups of PAA are covalently grafted to the amino groups of nylon 6,6 using a triazine-based condensing reagent, DMTMM. Since PAA is more hydrophilic than nylon, the water contact angle on PAA-grafted nylon film should be less than 72º. As shown in Table 5.1, the water contact angles measured on smooth PAA-grafted nylon film made as described in the experimental section were found to be $43º \leq \theta_e \leq 50º$. This is in good agreement with the values found by Thompson. Figure 5.2 shows a water droplet sitting on a PAA-grafted nylon film; the equilibrium water contact angle on this surface is 43º.

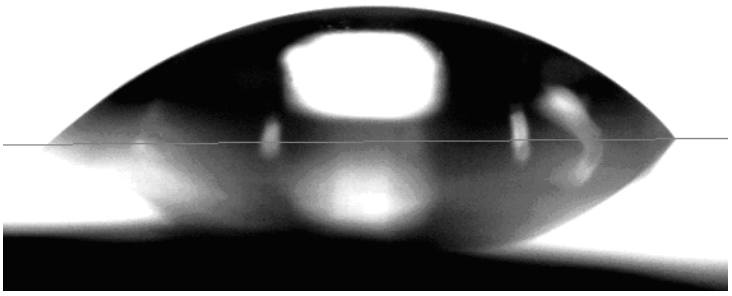

Figure 5.2. A water droplet on a PAA-grafted nylon surface. The water contact angle on this surface is 43º.

Next, to make the surface hydrophobic, 1H, 1H-perfluorooctylamine was grafted onto the PAA-grafted nylon films, again using DMTMM as a condensing agent following the procedures described by Thompson. When water is placed on a clean, smooth poly(tetrafluoroethylene) (PTFE) surface (γ_S^d = 18.5 dyne/cm), θ_e = 117º. The water contact angles measured on the 1H, 1H-perfluorooctylamine-grafted-PAA-grafted nylon films were 93º ≤ θ_e ≤ 110º (Table 5.1). These values are in agreement with those found by Thompson, but lower than expected for a fluorochemical surface. Thompson attributed this difference to incomplete coverage of the surface via grafting and showed that approximately 80% of the PAA is covered by fluoroamine. Thus, by chemically grafting 1H, 1H-perfluorooctylamine onto PAA that has previously been grafted to a nylon surface, the surface is rendered hydrophobic. We use this procedure to make our rough surface hydrophobic, as described below. Figure 5.3 presents a water droplet sitting on a 1H, 1H-perfluorooctylamine-grafted PAA-grafted nylon film; the water contact angle on this surface is 100º.

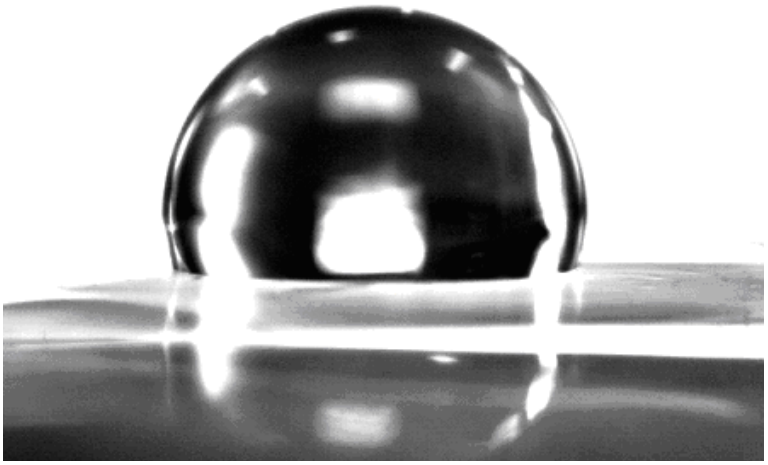

Figure 5.3. A water droplet on a 1H, 1H-perfluorooctylamine-grafted PAA-grafted nylon surface. The water contact angle on this surface is 100º.

In the same manner, to make the film surface hydrophobic, octadecylamine was grafted onto the PAA-grafted nylon films as described in the experimental section. Since octadecylamine is more hydrophobic than nylon due to the alkyl groups, θ_e should be greater than 73º and potentially as high as 110° for octadecylamine. The water contact angles measured on the octadecylamine-grafted PAA-grafted nylon film were $95º \leq \theta_e \leq 102º$ as shown in Table 5.1. Thus, the first criterion for making a superhydrophobic surface has been achieved.

5.2. Preparation of superhydrophilic rough surfaces

5.2.1. Superhydrophilic flock surfaces

The next step in the process of making a superhydrophilic material is to generate an appropriate rough surface. The predominant approach to model a superhydrophilic rough surface is the Wenzel model. According to the model, a surface of a composite material can be superhydrophilic when the material consists of a rough surface having appropriate roughness, r, as shown in equations (2.19). In this study, rod-shaped nylon flock fibers were attached on a polyester substrate. The protruding flock fibers can be thought of as pillars sticking up from the fabric surface as depicted in Figure 5.4.

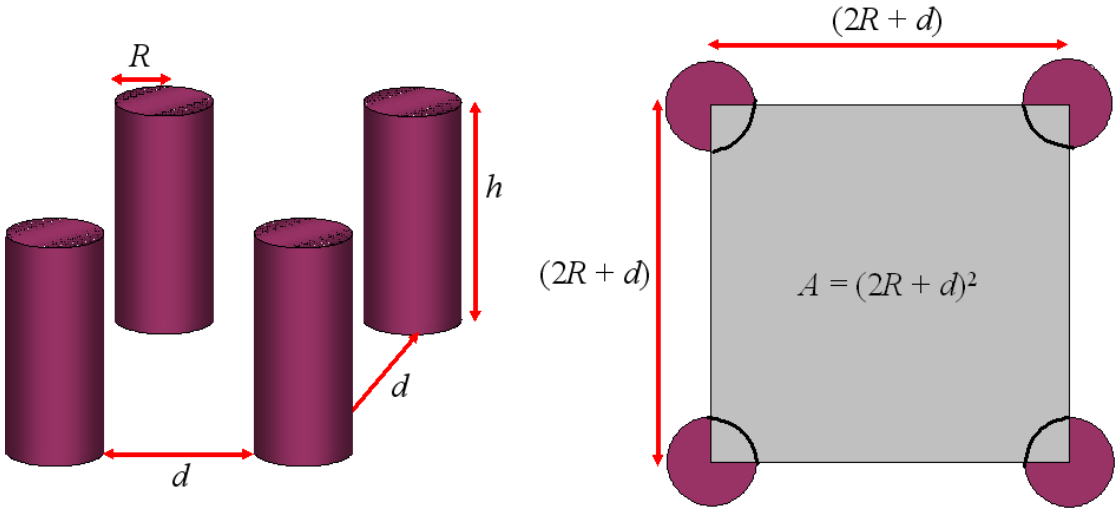

Figure 5.4. Side and upper views of roughness pattern.

For this rough surface, r is defined as:

$$r = \frac{2\pi Rh}{(2R+d)^2} + 1 \tag{5.1}$$

where R and h are the radius and height of a flock fiber, respectively; and d is the distance between two adjacent fibers. Reformulating the Wenzel equation gives:

$$\cos\theta_r^W = \left(\frac{2\pi Rh}{(2R+d)^2} + 1\right)\cos\theta_e \tag{5.2}$$

Four kinds of rough surfaces having different dimensions were fabricated. Table 5.2 describes the geometric parameters of the nylon fibers used to generate the rough surfaces. Each surface is identified as nylon flock, NF, and the height to radius ratio. For example, NF70 is made with nylon flock fibers with a height to radius ratio of 70.

Table 5.2. Dimensions of pillar shaped nylon flock fibers

Sample	Dimensions			
	dtex*	Radius** (μm)	Height (μm)	Height / Radius
NF50	3.3	10	500	50
NF70	1.7	7	500	70
NF100	3.3	10	1000	100
NF140	1.7	7	1000	140

* Linear density: 1 dtex = 1g / 10,000m

** Calculated from linear density of each fiber and density of nylon 6,6 (1.14 g/cm^3)

Table 5.3 shows the measured interfiber distances between adjacent fibers determined at 20 different locations. The Wenzel roughness, r, on each sample was calculated by using equation (5.2).

Table 5.3. Measured distances between two adjacent flock fibers and roughness, r

Sample	Measured distance* (μm)	Roughness, r
NF50	$5 \leq d \leq 120$	$2.6 \leq r \leq 51.3$
NF70	$10 \leq d \leq 120$	$2.2 \leq r \leq 39.2$
NF100	$25 \leq d \leq 76$	$7.8 \leq r \leq 32.0$
NF140	$10 \leq d \leq 78$	$6.2 \leq r \leq 77.4$

* Measured at twenty random spots

Figure 5.5 shows SEM images of the flocked surface of NF140. The fiber radii and heights are approximately 7 μm and 1 mm, respectively. Inter-fiber spacings were measured for adjacent fibers using Image J at 20 random locations. The distance between adjacent fibers ranged from 10 to 78 μm in Figure 5.5.

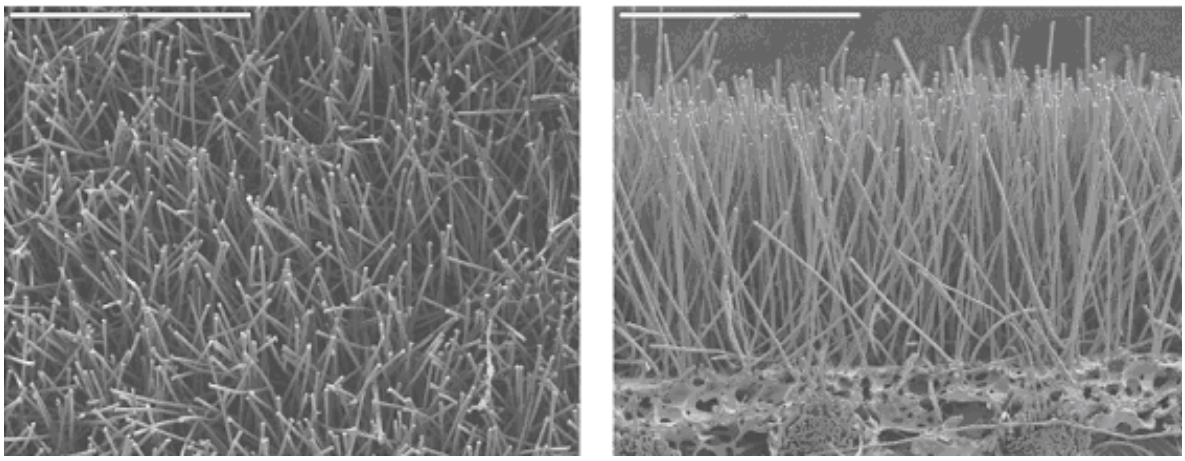

Figure 5.5. SEM views from above and from side of NF140 (50x).

Table 5.4 shows the predicted and measured water contact angles for the rough nylon structures made by flocking. For rough surfaces, the predicted water contact angles were obtained from both the Wenzel equation. According to the Wenzel equation, lower values of apparent contact angles are expected on rough surfaces when $\theta_e < 90^o$. For our rough surfaces, the water contact angles on nylon rough surfaces are predicted to be close to 0º. Indeed, rough surfaces made of nylon flock fibers absorb water into the flocked structure and the contact angles are 0° as expected. For the untreated nylon film and flocked fabrics the agreement between the predicted and measured contact angles is excellent. Figure 5.6 shows a water droplet absorbed into the fabric structure of nylon NF50. The apparent water contact angle on this surface approaches 0º.

Table 5.4. Comparison of predicted and measured apparent contact angles of superhydrophilic flock surfaces

Sample	Apparent contact angle (degree)			
	Nylon		PAA-grafted nylon	
	Predicted	Measured	Predicted	Measured
NF50	$\theta_r = 0$	$\theta_r \approx 0$	$\theta_r = 0$	$\theta_r \approx 0$
NF70	$\theta_r = 0$	$\theta_r \approx 0$	$\theta_r = 0$	$\theta_r \approx 0$
NF100	$\theta_r = 0$	$\theta_r \approx 0$	$\theta_r = 0$	$\theta_r \approx 0$
NF140	$\theta_r = 0$	$\theta_r \approx 0$	$\theta_r = 0$	$\theta_r \approx 0$

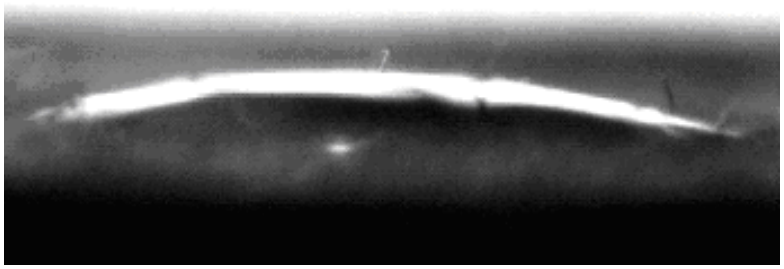

Figure 5.6. A water droplet on a nylon NF50 surface. The apparent water contact angle on this surface is close to 0º.

Upon treating the film surface with PAA, the water contact angle is expected to decrease. In the same manner, the water contact angles on a rough surface are expected to approach 0º. Indeed, the PAA-grafted nylon rough surfaces absorb water into the flocked

structure and the water contact angles of PAA-grafted rough surfaces are 0°. Again, excellent agreement is found between the predicted values of the apparent contact angle and the measured values when the contact angle follows the Wenzel model and θ_e is less than 90°. Figure 5.7 shows a water droplet completed immersed into the fabric structure of PAA-grafted nylon NF50. The apparent water contact angle on this surface is 0º.

Figure 5.7. A water droplet on a PAA-grafted nylon NF50 surface. The water contact angle on this surface is 0º.

5.2.2. Superhydrophilic plain woven surfaces

As mentioned in the introduction section, since $\cos\theta_r^W = r\cos\theta_e$, θ_r^W goes toward zero when $\theta_e < 90°$, and the liquid is sucked into contact with the rough surface. In other words, a hydrophilic surface becomes more hydrophilic when roughness, r, increases. Figure 5.8 shows a cross sectional view of a model of a plain woven fabric made from

monofilament yarns. The surface area of a single round monofilament yarn in the unit fabric can be calculated based on Figure 5.8.

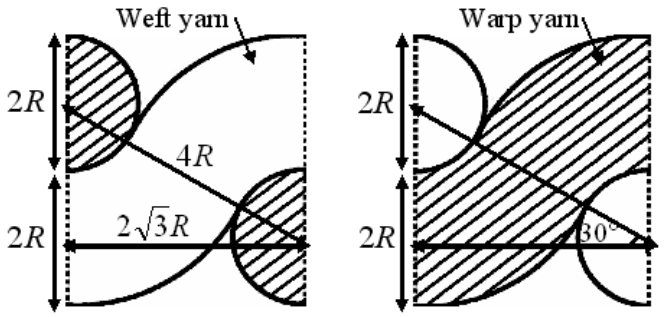

(a) (b)

Figure 5.8. The cross section views of a plain woven fabric: at the warp yarn direction (a) and at the weft yarn direction (b).

For this rough surface, r is defined using flux integral. As shown in Figure 5.8, the distance from the center of a weft yarn to the center of an adjacent weft yarn is $4R$; in the same manner, the distance from the center of a warp yarn to the center of an adjacent warp yarn is $4R$; and the distance from the center of a weft yarn to the center of an adjacent warp yarn is $2R$. Hence, according to Pythagorean theorem, the vector from the center of one weft yarn to the center of an adjacent weft yarn makes a 30° angle to the plane of the fabric. Using flux integral, the area of one yarn in the unit fabric is calculated as:

$$r(u,v) = (2R + R\cos v)\cos u\,i + (2R + R\cos v)\sin u\,j + R\cos v\,k$$

$$r_u = -(2R + R\cos v)\sin u\,i + (2R + R\cos v)\cos u\,j$$

$$r_v = -R\sin v\cos u\,i - R\sin v\sin u\,j + R\cos v\,k$$

$$r_u \times r_v = R(2R + R\cos v)\cos u\cos v\,i + R(2R + R\cos v)\sin u\cos v\,j + R(2R + R\cos v)\sin v\,k$$

$$\left| r_u \times r_v \right| = R(2R + R\cos v)$$

$$A_{yarn\ in\ unit\ area} = \frac{\int_0^{2\pi}\int_0^{2\pi} R(2R + R\cos v)dudv}{3}$$

$$A_{yarn\ in\ unit\ area} = \frac{8\pi^2 R^2}{3} = A_{weft\ yarn\ in\ unit\ area} = A_{warp\ yarn\ in\ unit\ area} \tag{5.3}$$

where R is the radius of yarn; A is the area; i, j and k are the vectors to x, y, and z axis direction, respectively; u and v are the notations for the variables of integration. Then, we determine the true fabric surface area as follows:

$$A_{fabric}^{real} = A_{weft\ yarn\ in\ unit\ area} + A_{warp\ yarn\ in\ unit\ area} \tag{5.4}$$

where A^{real}_{fabric} is the intrinsic area of the unit fabric determined by the area of yarn surfaces. We have two yarns in the unit area. Substituting equation (5.3) into equation (5.4) gives:

$$A_{fabric}^{real} = 52.64R^2 \tag{5.5}$$

The apparent surface area is just equal to the area of a plane tangent to the top surface.

$$A_{fabric}^{apparent} = 2\sqrt{3}R \times 2\sqrt{3}R = 12R^2 \tag{5.6}$$

where $A^{apparent}_{fabric}$ is the apparent area of the unit fabric shown in Figure 5.8. Finally, the roughness, r, is just the ratio of these areas:

$$r = \frac{A_{fabric}^{real}}{A_{fabric}^{apparent}} = \frac{52.64R^2}{12R^2} = 4.39 \tag{5.7}$$

In order to simplify the derivation of r, the circumference of a yarn is $2\pi R$. The length of the yarn in a unit cell is $4R$. So the surface area of a single round, monofilament

yarn in the unit cell is $8\pi R^2$. There are two yarns in a unit cell, one warp and one weft. Thus, the true surface area for the entire thickness of a monofilament plain woven fabric is $16\pi R^2$ as shown in equation (5.3). The apparent surface area is just equal to the area of a plane tangent to the top surface as shown in equation (5.6). Finally, the roughness, r, is just the ratio of these areas:

$$r = \frac{A_{fabric}^{real}}{A_{fabric}^{apparent}} \approx \frac{4}{3}\pi = 4.19 \tag{5.8}$$

On substituting $r = 4.19$, which is close to $r = 4.39$ derived by the flux integral, and the measured contact angles $65^o \leq \theta_e \leq 73^o$ on the flat nylon film and $43^o \leq \theta_e \leq 50^o$ on the flat PAA-grafted nylon film into equation (2.19), $\theta_r^W = 0^o$ for both fabrics regardless of PAA-grafting. The predicted values are in good agreement with the measured angles as shown in Table 5.5.

Table 5.5. Comparison of predicted and measured apparent contact angles of superhydrophilic woven surfaces

Sample	Apparent contact angle (degree)			
	Nylon		PAA-grafted nylon	
	Predicted	Measured	Predicted	Measured
Monofilament woven fabric	$\theta_r = 0$	$\theta_r \approx 0$	$\theta_r = 0$	$\theta_r \approx 0$
Multifilament woven fabric	$\theta_r = 0$	$\theta_r \approx 0$	$\theta_r = 0$	$\theta_r \approx 0$

Next, we look at a plain woven fabric made with multifilament yarns. Clearly, a multifilament yarn will have even higher values of r, since the space between the fibers will increase the real surface area while the apparent surface area remains the same. In this case, equation (5.3) becomes:

$$A_{fabric}^{real} = A_{multi} \approx 52.64R \times NR_f \tag{5.9}$$

where N is the number of filament fibers, R is the radius of the yarn, and R_f is the radius of the filament fibers. Substituting equation (5.9) into equation (5.7) yields:

$$r = \frac{A_{fabric}^{real}}{A_{fabric}^{apparent}} \approx \frac{4\pi NR_f}{3R} = 4.39\frac{NR_f}{R} \tag{5.10}$$

When $N = 1$, $R_f = R$. Otherwise, $R_f < R$ but $NR_f > R$. Figure 5.9 shows a plain woven fabric consisting of nylon 6,6 multifilament yarns. For this fabric, $R \approx 150$ μm, $N > 70$, and $R_f \approx 10$ μm. Substituting these values into equation (5.10) gives $r > 20.48$.

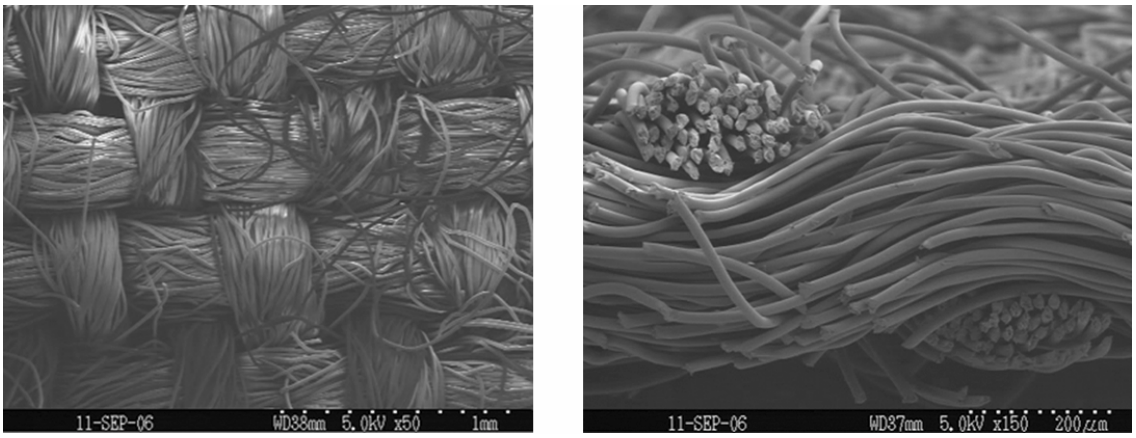

Figure 5.9. SEM micrographs of a multifilament plain woven fabric.

Since $r > 20.48$ for the multifilament fabric, we again expect that $\theta_r^W = 0º$ for both the nylon fabric and the PAA-grafted fabric. Again the predicted values are in good agreement with the measured angles as shown in Table 5.5. Thus, we can easily create Wenzel type behavior with complete wetting by having $\theta_e < 90°$ and sufficient roughness. Figure 5.10 shows a water droplet completed absorbed into the structure of nylon multifilament plain woven fabric. The apparent water contact angle on this surface is 0º.

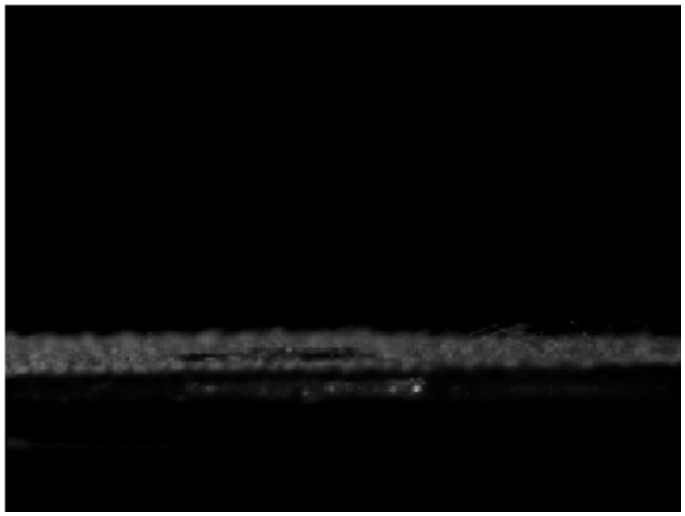

Figure 5.10. A water droplet absorbed into plain woven structure made of nylon multifilament fibers. The water contact angle on this surface is 0º.

5.2.3. Modeling of other superhydrophilic woven surfaces

As mentioned in the previous section, the apparent contact angle goes toward zero when the equilibrium contact angle on a smooth surface is less than 90° and the surface is roughened. The liquid on a rough surface is absorbed into contact with the rough surface and the hydrophilic surface becomes more hydrophilic. Figure 5.11 shows a cross sectional view of a model of a 2/1 twill woven fabric made from monofilament yarns. The surface area of a single round monofilament yarn in the unit fabric can be calculated based on Figure 5.11 using flux integral in order to obtain *r*.

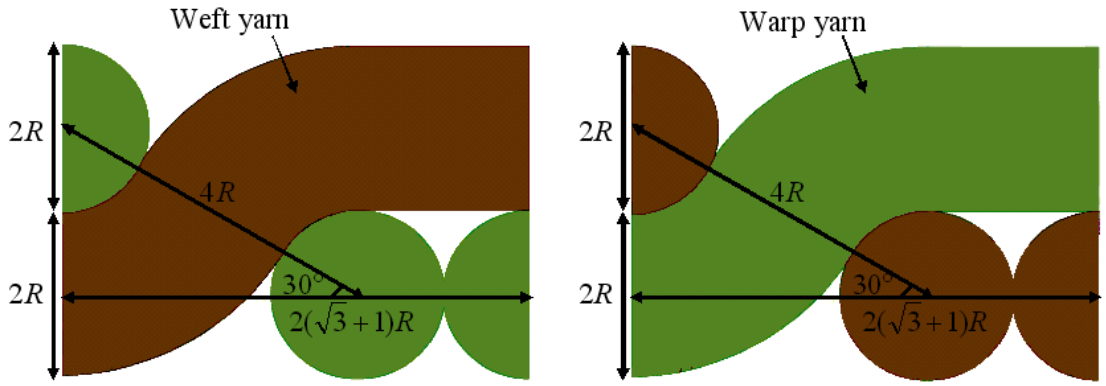

Figure 5.11. The cross section views of a 2/1 twill woven fabric.

As shown in Figure 5.8, the distance from the center of a weft (or warp) yarn to the center of an adjacent weft (or warp) yarn is 4*R*, and the distance from the center of a weft (warp) yarn to the center of an adjacent warp (weft) yarn is 2*R*. Hence, the vector from the center of one weft yarn to the center of an adjacent weft yarn, or the vector from the center of one warp yarn to the center of an adjacent warp yarn, makes a 30° angle to the plane of the fabric, as the plain woven fabric does. Therefore, the area of one yarn in the unit fabric is calculated as:

$$A_{yarn\ in\ unit\ area} = \frac{\int_0^{2\pi}\int_0^{2\pi} R(2R + R\cos v)dudv}{3} + \pi R^2$$

$$A_{yarn\ in\ unit\ area} = (\frac{8\pi^2}{3} + \pi)R^2 = A_{weft\ yarn\ in\ unit\ area} = A_{warp\ yarn\ in\ unit\ area} \quad (5.11)$$

Then, we determine the true fabric surface area as follows.

$$A_{fabric}^{real} = A_{weft\ yarn\ in\ unit\ area} + A_{warp\ yarn\ in\ unit\ area} = 2(\frac{8\pi^2 + \pi}{3})R^2 \quad (5.12)$$

where A^{real}_{fabric} is the intrinsic area of the unit fabric determined by the area of yarn surfaces. We have four yarns in the unit area. Therefore, the real fabric area is:

$$A^{real}_{fabric} = 4(52.64 + 2\pi)R^2 = 218.82R^2 \tag{5.13}$$

The apparent surface area is just equal to the area of a plane tangent to the top surface.

$$A^{apparent}_{fabric} = 2R(\sqrt{3}+1) \times 2R(\sqrt{3}+1) = 29.85R^2 \tag{5.14}$$

where $A^{apparent}_{fabric}$ is the apparent area of the unit fabric shown in Figure 5.11. Finally, the roughness, *r*, is just the ratio of these areas:

$$r = \frac{A^{real}_{fabric}}{A^{apparent}_{fabric}} = \frac{218.82R^2}{29.85R^2} = 7.33 \tag{5.15}$$

Since $r = 7.33$, and the measured contact angles $65^o \leq \theta_e \leq 73^o$ on the flat nylon film and $43^o \leq \theta_e \leq 50^o$ on the flat PAA-grafted nylon film into equation (2.19), $\theta_r^W = 0^o$ for both fabrics regardless of PAA-grafting. Indeed, the predicted values were in good agreement with the measured angles although we reformed the 2/1 twill woven surface, which was calendered by heat, was used for this experiments (Table 5.5).

In the same manner, the Wenzel roughness, *r*, of 3/1 twill fabrics can be obtained. Figure 5.12 shows a cross sectional view of a model of a 3/1 twill woven fabric made from monofilament yarns. The surface area of a single round monofilament yarn in the unit fabric can be calculated based on Figure 5.12.

.

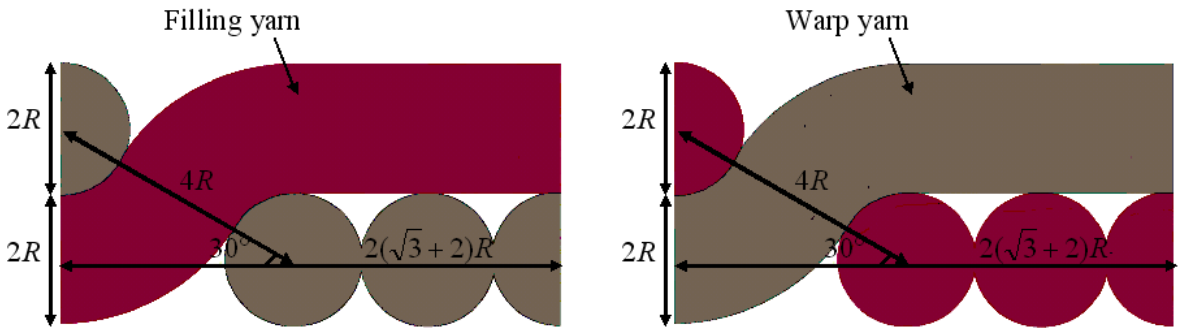

Figure 5.12. The cross section views of a 3/1 twill woven fabric.

The area of one yarn in the unit fabric is calculated as:

$$A_{yarn\ in\ unit\ area} = \frac{\int_0^{2\pi}\int_0^{2\pi} R(2R + R\cos v)dudv}{3} + 2\pi R^2$$

$$A_{yarn\ in\ unit\ area} = (\frac{8\pi^2}{3} + 2\pi)R^2 = A_{weft\ yarn\ in\ unit\ area} = A_{warp\ yarn\ in\ unit\ area} \quad (5.16)$$

Then, we determine the true fabric surface area as follows:

$$A_{fabric}^{real} = A_{weft\ yarn\ in\ unit\ area} + A_{warp\ yarn\ in\ unit\ area} = 2(\frac{8\pi^2 + 2\pi}{3})R^2 \quad (5.17)$$

where A^{real}_{fabric} is the intrinsic area of the unit fabric determined by the area of yarn surfaces. We have six yarns in the unit area. Therefore, the real fabric area is:

$$A_{fabric}^{real} = 6(52.64 + 2\pi)R^2 = 353.59R^2 \quad (5.18)$$

The apparent surface area is just equal to the area of a plane tangent to the top surface.

$$A_{fabric}^{apparent} = 2R(\sqrt{3} + 2) \times 2R(\sqrt{3} + 2) = 55.71R^2 \quad (5.19)$$

where $A^{apparent}_{fabric}$ is the apparent area of the unit fabric shown in Figure 5.12. Finally, the roughness, *r*, is just the ratio of these areas:

$$r = \frac{A_{fabric}^{real}}{A_{fabric}^{apparent}} = \frac{353.59R^2}{55.71R^2} = 6.35 \tag{5.20}$$

The Wenzel roughness of 3/1 twill fabric, r = 6.35, was derived by the flux integral. Since the measured contact angles of both nylon and PAA-grafted nylon film are less than 90º, the apparent contact angles, θ_r^W, are equal to 0º for both fabrics. In addition, with comparing equation (5.20) to equation (5.15), the roughness of woven fabrics decreases when the structures have longer floats than a 2/1 twill.

5.3. Preparation of superhydrophobic rough surfaces

5.3.1. Superhydrophobic flock surfaces

The next step in the process of making a superhydrophobic material is to take the rough surfaces and make them hydrophobic. The predominant approach of modeling a superhydrophobic rough surface is the Cassie-Baxter model. According to this model, a surface of a composite material can be superhydrophobic when the material consists of a rough surface having the appropriate area fraction of the surface in contact with water, Φ_S, as shown in equations (2.27). In this study, rod-shaped nylon flock fibers were attached on a polyester substrate. The protruding flock fibers can be thought of as pillars sticking up from the fabric surface as depicted in Figure 5.4.

For this rough surface, Φ_S is defined as:

$$\Phi_S = \frac{\pi R^2}{(2R+d)^2} \tag{5.21}$$

where R and h are the radius and height of a flock fiber, respectively; and d is the distance between two adjacent fibers. Reformulating the Cassie-Baxter equations gives:

$$\cos\theta_r^{CB} = \frac{\pi R^2}{(2R+d)^2}(\cos\theta_e + 1) - 1 \tag{5.22}$$

Figure 5.13 shows the region of the wetted area fraction, Φ_S, for the development of a superhydrophobic surface ($\theta_r \geq 150°$) when a rough surface is covered by a low surface

tension material such as poly(tetrafluoroethylene, PTFE) ($\theta_e \approx 119°$). The graph shows that this rough surface becomes superhydrophobic when $\Phi_S \leq 26\%$.

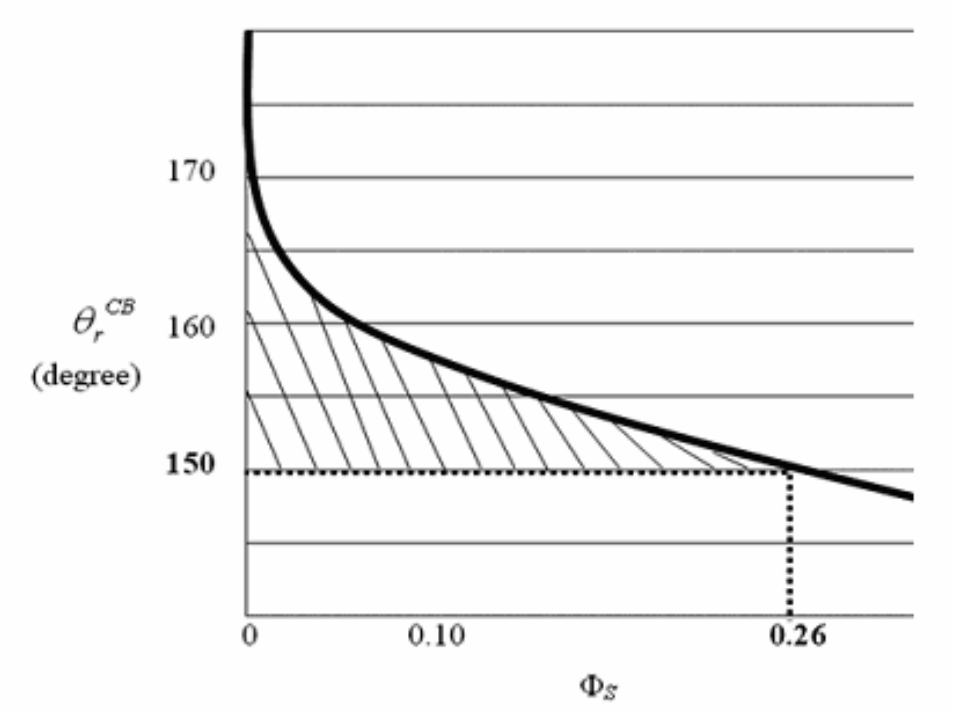

Figure 5.13. Plots of apparent water contact angles on a fluoroamine covered rough surface in Cassie-Baxter model; Crosshatched area indicates the superhydrophobic region.

Four kinds of rough surfaces having different dimensions were fabricated as before. If the surface of these fibers is modified to have a surface tension of 18.5 dyne/cm, equation (5.22) predicts the surface will be superhydrophobic if the adjacent fibers have the spacings listed in Table 5.6. This table shows the interfiber distances measured on adjacent fibers at 20 different locations on each sample and the top area fractions, Φ_S.

Table 5.6. Measured distances between two adjacent flock fibers and top area fraction, Φ_S

Sample	Measured distance* (μm)	Top area fraction, Φ_S
NF50	$5 \leq d \leq 120$	$0.02 \leq \Phi_S \leq 0.50$
NF70	$10 \leq d \leq 120$	$0.01 \leq \Phi_S \leq 0.26$
NF100	$25 \leq d \leq 76$	$0.03 \leq \Phi_S \leq 0.16$
NF140	$10 \leq d \leq 78$	$0.02 \leq \Phi_S \leq 0.26$

* Measured at twenty random spots

According to Table 5.6, all the samples have potential to be superhydrophobic when the surfaces are grafted with 1H, 1H-perfluorooctylamine. Indeed, fluoroamine modified NF70, NF100 and NF140 are superhydrophobic with apparent water contact angles are over 150°, as shown in Table 5.7. For rough surfaces, the predicted water contact angles were obtained from equation (2.27).

Table 5.7. Comparison of predicted and measured apparent contact angles of hydrophobic and superhydrophobic flock surfaces

Sample	Apparent contact angle (degree)	
	Predicted	Measured
NF50	$122 \leq \theta_r \leq 171$	$132 \leq \theta_r \leq 140$
NF70	$139 \leq \theta_r \leq 173$	$168 \leq \theta_r \leq 175$
NF100	$148 \leq \theta_r \leq 169$	$170 \leq \theta_r \leq 178$
NF140	$140 \leq \theta_r \leq 171$	$170 \leq \theta_r \leq 178$

The Cassie-Baxter model predicts that a rough surface becomes more hydrophobic when Φ_S decreases. Upon further treatment of the PAA-grafted nylon film with 1H, 1H-perfluorooctylamine, the contact angle of water on the flat film increases to $\theta_e = 93° \sim 110°$. Thus the 1H, 1H-perfluorooctylamine-grafted rough surfaces should be more hydrophobic ($\theta_r > \theta_e$) when the surface is roughened. This is exactly what is observed for all of our rough surfaces. Samples NF70, NF100, and NF140 are all superhydrophobic ($\theta_r \geq 150°$) when 1H, 1H-perfluorooctylamine is grafted to the surfaces. For example, NF 100 and NF140 have high apparent contact angles, $170° \sim 178°$, and are superhydrophobic. Figure 5.14 shows a water droplet sitting on 1H, 1H-perfluorooctylamine grafted NF70. The water contact angle in this image seems to be 175°. Light can be seen between the droplet and a

rough surface, which indicates that the water droplet is sitting on the top of flock fibers and follows the Cassie-Baxter model.

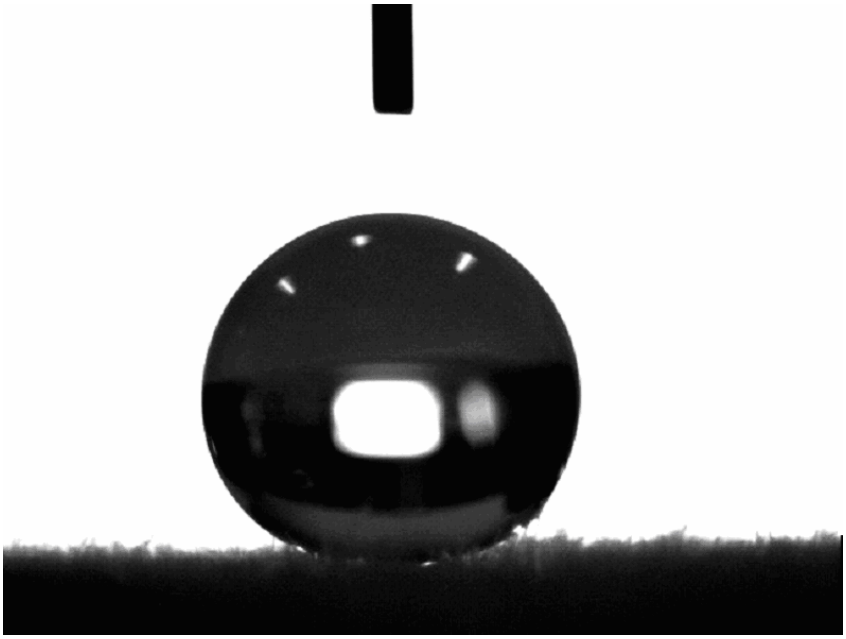

Figure 5.14. A water droplet on a superhydrophobic surface of NF70. Lights under the droplet show that water is sitting on the top of the flock fibers.

Although NF50 made of 1H, 1H-perfluorooctylamine-grafted nylon flock fibers has the potential to be superhydrophobic, the measured contact angle is less than 150º. In addition, the measured water contact angles of NF70, NF100, and NF140 are slightly outside of the range predicted in Table 5.7. This result shows the simplified Cassie-Baxter equation is not for the design of a superhydrophobic surface when the top of a rough surface is not completely flat after the surface is roughened. In next section we use the original Cassie-Baxter equation to overcome this challenge.

5.3.2. Superhydrophobic woven surfaces

To make a superhydrophobic surface, we first need to make the surface hydrophobic and create the appropriate roughness. According to Cassie and Baxter, and Marmur, and as is evident from equations (2.25) and (2.30), the Wenzel model is a special case of the Cassie-Baxter equation where $f = 1$ and $r_f = r$ (equation 2.30). For a material with a smooth surface water contact angle of 93° (as above), the Wenzel surface roughness, r, must be greater than 16.5 for the apparent contact angle to exceed 150°. However, according to Marmur, the minimization of the free energy requires that, for a hydrophobic surface with $f = 1$, $\theta_e = 180°$. Since the only material known with $\theta_e = 180°$ is air or vacuum, f cannot be equal to one. In other words, the Wenzel model is invalid for hydrophobic surfaces. In order to develop superhydrophobic surfaces, we need to use a different approach, namely the Cassie-Baxter model.

We begin with an analysis of f, the fraction of the projected area in contact with the water droplet. For parallel cylinders viewed normal to the cylinders' axes there are two cases (a) the cylinders are packed tightly together, or (b) they are separated by some distance, as shown in Figure 5.15. In case (a), the distance from the center on one cylinder to the center of the next is $2R$, where R is the radius of the cylinder. In case (b), by analogy, the center-to-center distance is considered to be $2(R + d)$. In case (a), Marmur showed that $f = \sin\alpha$ where α is the angle between the top of the cylinder and the liquid contact line and $\alpha = \pi - \theta_e$. In case (b), $f = R \sin\alpha / (R + d)$; and in both cases, $r_f = \alpha / \sin\alpha$. Therefore, using

simple differentials we obtain $d(r_f f) / dr_f = (\cos\alpha)^{-1}$ and $d(r_f f)^2 / dr_f^2 > 0$ in both (a) and (b). According to Marmur, under these conditions, there is a minimum surface free energy on each surface such that $\alpha = \pi - \theta_e$. Substituting for f and r_f for case (b) into equation (2.30) results in:

$$\cos\theta_r^{CB} = -\left(\frac{R}{R+d}\right)\alpha\cos\alpha + \left(\frac{R}{R+d}\right)\sin\alpha - 1 \tag{5.23}$$

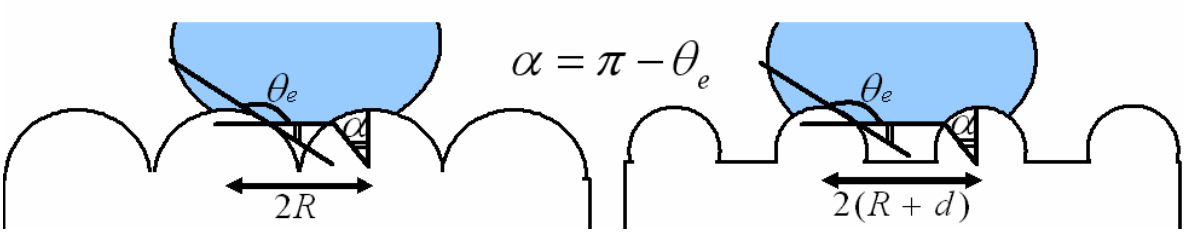

(a) (b)

Figure 5.15. A liquid drop sitting on (a) cylinders packed tightly, and (b) cylinders separated by a distance, $2d$. $\alpha = \pi - \theta_e$.

On substituting $\pi - \theta_e$ for α, we obtain:

$$\cos\theta_r^{CB} = \left(\frac{R}{R+d}\right)(\pi - \theta_e)\cos\theta_e + \left(\frac{R}{R+d}\right)\sin\theta_e - 1 \tag{5.24}$$

For $\theta_e > 90°$, θ_r^{CB} increases with increasing d. For example, when $\theta_e = 120°$ and $d = 0$, the fibers are closely packed and $\theta_r^{CB} = 131°$; for $d = R$, $\theta_r^{CB} = 146°$; and for $d = 2R$, $\theta_r^{CB} = 152°$.

We consider two cases for solving equation (5.24). First we solve it for a monofilament plain woven fabric shown in Figure 5.8. Again, according to Pythagorean's

theorem, the angle that a weft yarn (or warp yarn) makes with the fabric plane in traveling from one warp yarn (or weft yarn) to another is 30°. Therefore, the distance from the top of a weft yarn (or warp yarn) to the top of an adjacent warp yarn (or weft yarn) is $2\sqrt{3}R$. From this geometric consideration, the center-to-center distance of adjacent cylinders in equation (5.24), $2(R + d)$, is equal to $2\sqrt{3}R$, and $f = \sin\alpha / \sqrt{3}$. Substituting these values into equation (5.24) along with the measured contact angles from the flat nylon films, we find $118° \le \theta_r^{CB} \le 134°$ for the 1H, 1H-perfluorooctylamine-grafted monofilament woven fabric and $120° \le \theta_r^{CB} \le 127°$ for the octadecylamine–grafted monofilament woven fabric. These values are in good agreement with the measured values shown in Table 5.8.

Table 5.8. Comparison of predicted and measured apparent contact angles of hydrophobic and superhydrophobic woven surfaces

Sample	Apparent contact angle (degree)			
	1H, 1H-perfluorooctylamine-grafted nylon woven fabric		Octadecylamine-grafted nylon woven fabric	
	Predicted	Measured	Predicted	Measured
Monofilament woven fabric	$118 \leq \theta_r \leq 134$	$130 \leq \theta_r \leq 138$	$120 \leq \theta_r \leq 127$	$125 \leq \theta_r \leq 134$
Multifilament yarn	$123 \leq \theta_r \leq 138$	N/M*	$125 \leq \theta_r \leq 131$	N/M
Multifilament woven fabric	$146 \leq \theta_r \leq 158$	$160 \leq \theta_r \leq 168$	$147 \leq \theta_r \leq 152$	$155 \leq \theta_r \leq 168$
Calendered woven fabric	$112 \leq \theta_r \leq 127$	$109 \leq \theta_r \leq 113$	$114 \leq \theta_r \leq 120$	$107 \leq \theta_r \leq 110$

* Not measured

In the second case, we again extend the analysis to a multifilament fabric. We begin by determining the apparent contact angle of the liquid with the multifilament yarns. From Figure 5.9, it is seen that the fiber spacing is approximately equal to the fiber diameter, i.e. $2d \approx 2R_f$, where R_f is the fiber radius. Substituting R_f for R and d into equation (5.24), as shown in Table 5.8, we obtain θ_r^{CB} ranging from 123° to 138° for the 1H, 1H-perfluorooctylamine-grafted single fiber, and from 125° to 131° for the octadecylamine-grafted single fiber. Then, using these values as the effective contact angles for the yarns in the woven structure and re-solving equation (5.24) with R being the yarn radius and

$d = R(\sqrt{3} - 1)$ such that $2(R + d) = 2\sqrt{3}R$ as before. We obtain $146° \leq \theta_r^{CB} \leq 158°$ for the 1H, 1H-perfluorooctylamine-grafted fabric, and $147° \leq \theta_r^{CB} \leq 152°$ for the octadecylamine-grafted fabric. As seen in Table 5.8, the measured values are slightly larger than our predicted values. This is probably due to the real value of d being larger than the values chosen in this analysis. For example, the surface of the fabric shown in Figure 5.9 clearly has loose fibers on the surface that are not entrained in the yarn. These surface fibers are separated from the remainder of the fibers by distances $d > R$. As shown earlier, larger values of d result in larger values of θ_r^{CB}. Thus the measured values of θ_r^{CB} are greater than predicted values. Figure 5.16 shows a water droplet sitting on this surface; the apparent water contact angle on this surface is 168º.

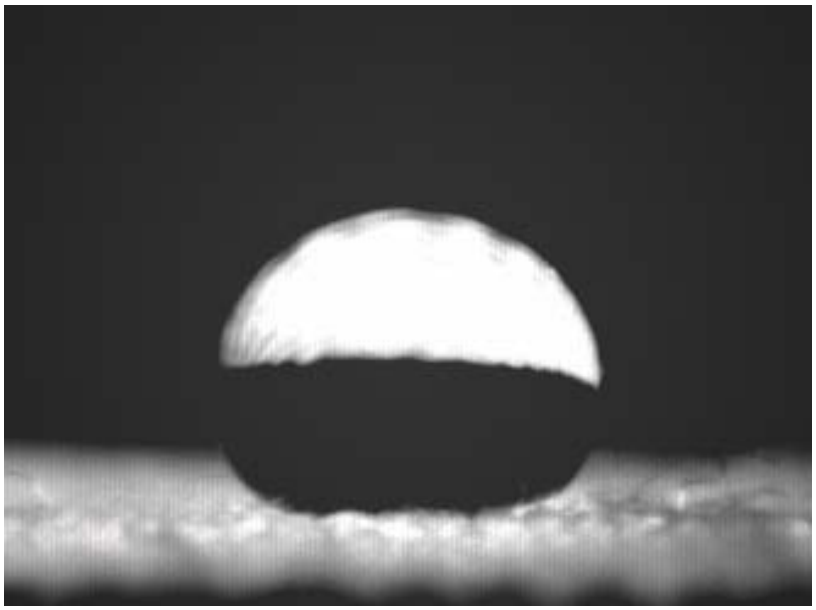

Figure 5.16. A water droplet on a multifilament plain woven fabric. The apparent water contact angle on this rough surface is 168º.

Others have reported the Cassie-Baxter model using equation (2.21). This form of the Cassie-Baxter equation is valid only when a surface is perfectly smooth (i.e. $\Phi_S = r = 1$) or when the top of a rough surface is flat. Comparing equation (2.21) to equations (2.25) and (2.30) shows that equation (2.25) is only correct when $f_1 + f_2 = 1$. However, $f_1 + f_2 > 1$ on general rough surfaces. For example, in the multifilament yarns of Figure 5.9, $d = R(\sqrt{3} - 1)$, $\theta_e \approx 100°$ giving $f_1 = 0.81$ and $f_2 = 0.43$ since:

$$f_1 = \frac{R}{R + d}(\pi - \theta_e) \tag{5.25}$$

$$f_2 = 1 - \frac{R}{R + d}\sin\theta_e \tag{5.26}$$

Thus, in this case, $f_1 + f_2 = 1.24$. This is clearly not equal to one and equation (2.21) cannot be applied in this case. Rather, the original Cassie-Baxter equation is preferred.

An additional surface structure was analyzed using flattened fibers, which resulted in a smoother fabric. Figure 5.17 shows another woven fabric made of monofilament yarns that have been calendered. In this case, the fraction of the surface in contact with water, f_1, must be larger than that of round fibers since water will contact more of the surface of these flattened yarns. $f_1 + f_2$ is also greater than one on this rough surface. Since it is difficult to measure f_1 and f_2 of calendered fabric directly or to compute it from a simple fabric model, we estimated them through analyzing r_f and f from equations (2.28) and (2.29).

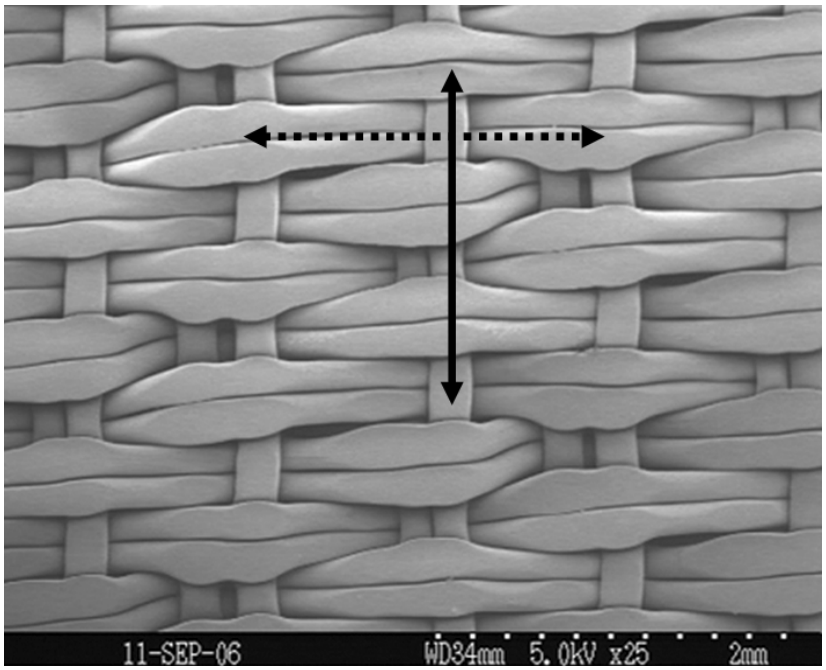

Figure 5.17. SEM micrograph of a calendered monofilament woven fabric. The solid line shows the warp direction, and the dotted line shows the weft direction.

The arrangement of the flattened fibers in this woven fabric is anisotropic. There are two types of fibers which can be regarded as flattened cylinders in this structure: cylinders passing through the warp direction shown as a solid line in Figure 5.17, and cylinders passing through the weft direction shown as a dotted line. As shown in Figure 5.17, only the cylinders passing through weft direction reside on the top of this rough surface. Thus, only these fibers are considered to obtain f and r_f. These top fibers have shorter center-to-center distance when measured in the warp direction (solid line) than when measured in the weft direction (dotted line). We measure R, b and d, which are defined in Figure 5.18, to obtain only the warp directional f and r_f. R is the radius of rounded part of a flattened cylinder, $2d$ is the spacing between the edges of the fibers, and $2b$ is the width of the

flattened portion of the fiber. Figure 5.18 presents the cross view of the unit structure of the fabric when it is cut through the solid line in Figure 5.17.

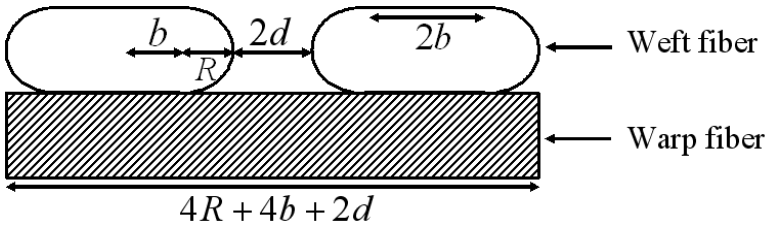

Figure 5.18. The cross unit section view of a calendered woven fabric shown in Figure 5.17 when it is cut to warp direction.

In the warp direction, two flattened cylinders are placed on the top of the rough surface at a distance, 2*d*, with the adjacent cylinders lying in the same direction. Thus, the unit center-to-center distance is 4(*R* + *b*) + 2*d* as shown in Figure 5.18. Since *f* is the fraction of the projected area of the rough surface that is wet by the liquid and r_f is the roughness ratio of the wet area, we obtain:

$$f = \frac{4b + 4R\sin\alpha}{4b + 2d + 4R} \tag{5.27}$$

$$r_f = \frac{4b + 4R\alpha}{4b + 4R\sin\alpha} \tag{5.28}$$

where α is the angle between the top of the cylinder and the liquid contact line ($\alpha = \pi - \theta_e$), Again, according to Marmur, the surface has a minimum surface free energy for θ_r^{CB}, when $d(r_f f) / dr_f = (\cos\alpha)^{-1}$ and $d(r_f f)^2 / dr_f^2 > 0$. Since $0 \le \alpha \le 90$, we obtained:

$$\frac{d(r_f f)}{dr_f} = \frac{d(\frac{4b + 4R\alpha}{4b + 4R + 2d})}{d(\frac{4b + 4R\sin\alpha}{4b + 4R + 2d})} = \frac{d(b + R\alpha)}{d(b + R\sin\alpha)} = \frac{1}{\cos\alpha} \tag{5.29}$$

$$\frac{d^2(r_f f)}{dr_f{}^2} = \frac{d(\cos^{-1}\alpha)}{d(\frac{4b + 4R\sin\alpha}{4b + 4R + 2d})} = \frac{\sin\alpha}{R(4b + 4R + 2d)\cos^3\alpha} > 0 \tag{5.30}$$

According to Marmur's analysis, the fabric in Figure 5.17 can have minimum in the free energy at the Cassie-Baxter apparent contact angle.

On substituting equations (5.27) and (5.28) into equations (2.23) and (2.24), f_1 and f_2 are obtained as:

$$f_1 = r_f f = \frac{4b + 4R\alpha}{4b + 4R + 2d} \tag{5.31}$$

$$f_2 = 1 - f = 1 - \frac{4b + 4R\sin\alpha}{4b + 4R + 2d} \tag{5.32}$$

On substituting equations (5.31) and (5.32) into equation (2.20);

$$\cos\theta_r^{CB} = \frac{b + R(\pi - \theta_e)}{b + R + 0.5d}\cos\theta_e + \frac{b + R\sin(\pi - \theta_e)}{b + R + 0.5d} - 1 \tag{5.33}$$

Using the SEM image of the rough surface, b, R, and d were measured at ten locations on the surface: b_{average} = 60 μm, R_{average} = 40 μm, and d_{average} = 100 μm. Applying the measured θ_e, b, R, and d to equation (5.33) gives 112° ≤ θ_r^{CB} ≤ 127° for the 1H, 1H-perfluorooctylamine-grafted nylon calendered monofilament fabric and 114° ≤ θ_r^{CB} ≤ 120° for the octadecylamine-grafted nylon calendered monofilament fabric. Although d of the

rough surface has a large coefficient of variation, about 30%, the predicted values show good agreement with the measured values, $109° \leq \theta_r^{CB} \leq 113°$ and $107° \leq \theta_r^{CB} \leq 110°$, respectively. As predicted by equation (5.33), this surface is not superhydrophobic due to the short distances between adjacent fibers and high portion of flat top surfaces.

5.3.3. Contact angle hysteresis and roll-off angle

Another portion of the definition of superhydrophobic materials is that they have a water roll-off angle of less than 5°. As shown in equation (2.32), repeated below, the roll-off angle depends on the size of the water droplet, the interfacial surface tension between liquid and vapor, and contact angle hysteresis. i.e. $\sin\alpha$ is proportional to the difference between $\cos\theta_A$ and $\cos\theta_R$. The roll-off angles of 1H, 1H-perfluorooctylamine-grafted and octadecylamine-grafted superhydrophobic nylon surface having multifilament nylon fibers were measured and compared to the predicted angles as shown in Table 5.9.

$$mg\sin\alpha \approx -2R\gamma_{LV}(\cos\theta_A - \cos\theta_R) \tag{2.32}$$

Table 5.9. Comparison of predicted and measured roll-off angles of superhydrophobic woven surfaces

Sample	Water volume (μL)	Roll-off angle (degree)	
		Predicted	Measured
1H, 1H-perfluorooctylamine-grafted nylon fabric	10	$13.37 \leq \alpha \leq 22.59$	$\alpha \geq 90$
	20	$8.38 \leq \alpha \leq 14.00$	$75 \leq \alpha \leq 90$
	50	$4.54 \leq \alpha \leq 7.54$	$20 \leq \alpha \leq 35$
	500	$0.97 \leq \alpha \leq 1.62$	$\alpha \leq 5$
Octadecylamine-grafted nylon fabric	10	$13.37 \leq \alpha \leq 28.51$	$\alpha \geq 90$
	20	$8.38 \leq \alpha \leq 17.50$	$55 \leq \alpha \leq 90$
	50	$4.54 \leq \alpha \leq 9.39$	$27 \leq \alpha \leq 53$
	500	$0.97 \leq \alpha \leq 2.02$	$\alpha \leq 5$

It is important that the droplet size must be much larger than the underlying structure in order to have a low roll-off angle. For our samples, the advancing contact angles of the 1H, 1H-perfluorooctylamine-grafted or octadecylamine-grafted multifilament fabric surface became very close to 180° when the droplet began to move. However, the receding contact angles were affected by the local structures of fabric such as protruding yarns, yarn size and yarn spacing on the surface. Although the receding contact angles were as small as 90°, the roll-off angles of these superhydrophobic surfaces were less than 5°

when a 0.5 mL water droplet was applied. However, when 10, 20, and 50 μL drops were applied, the roll-off angles were greater than 5° since the roll-off angle was influenced by the droplet size and local yarn or fabric geometry. When the droplet size approaches the underlying structure size, the assumptions in the Cassie-Baxter model begin to fail. Therefore, roll-off angles are affected by the local structures of fabric such as protruding yarns, yarn size and yarn spacing on the surface. Figure 5.18 shows the protruding fibers and the yarn size compared to the drop size.

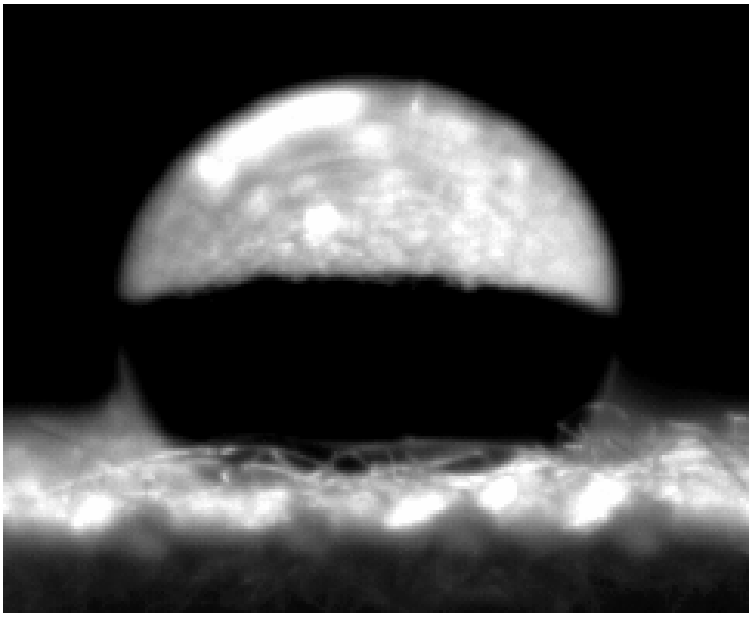

Figure 5.19. A 10 μL water droplet on a multifilament woven fabric.

6. CONCLUSION

In this paper, the wetting behavior on a flat surface was compared to that of a rough surface; the effect of the sliding angles of water droplet was analyzed; and the contact angle hysteresis on superhydrophobic surfaces was studied.

6.1. Design and development of superhydrophobic flock fabrics

In order to make nylon 6,6 superhydrophobic, a low surface energy material, 1H, 1H-perfluorooctylamine, was grafted onto rough surfaces of nylon 6,6, which were made by flocking and water contact angles were measured. The rough surface became more hydrophobic than the corresponding flat surface when $\theta_e > 90°$ but more hydrophilic when $\theta_e < 90°$. Since nylon and PAA are hydrophilic, rough surfaces made of nylon or the PAA grafted nylon absorbed water into the structures, and both surfaces became more hydrophilic. However, the nylon rough surface grafted with a low surface energy material, 1H, 1H-perfluorooctylamine, became superhydrophobic ($\theta_r \geq 150°$) when inter-fiber distances between adjacent fibers fell within the ranges predicted by the Wenzel and the Cassie-Baxter models. Surfaces with water contact angles as high as 178° were made. Both mechanical and chemical surface modifications were required to make superhydrophobic surfaces.

6.2. Design and development of superhydrophobic woven fabrics

A superhydrophobic surface is obtained by two criteria: a low surface energy and an appropriate surface roughness which results in water detaching from the surface at a low roll-off angle. In order to make nylon 6,6 superhydrophobic, a low surface tension material, 1H, 1H-perfluorooctylamine or octadecylamine was grafted onto nylon 6,6 woven fabric consisting of multifilament yarns. We modeled the multifilament, plain woven fabric as consisting of monofilaments whose water contact angle was equal to the apparent water contact angle of the multifilament yarn. We approximated the fabric as parallel cylinders with radii equal to that of the multifilament yarns. From the water contact angles measured on flat, modified nylon films, we predicted the apparent contact angle of the woven fabrics. Good agreement between the predicted values and the observed contact angles was obtained. Apparent water contact angles of the multifilament woven fabric as high as 168° were obtained. A flattened fabric was also modeled and the predicted and measured values for this fabric also were in good agreement. It is important to note that the form of the Cassie-Baxter equation in common use today is generally invalid, and the original Cassie-Baxter equation or the reformulated Cassie-Baxter equation by Marmur have to be used when the top of a rough surface is not completely flat.

When the droplet began to roll off, the advancing contact angles of superhydrophobic woven surfaces became very close to 180° and the receding contact angles were as small as 90° since the receding angles were affected by the local structures

of fabric such as protruding yarns, yarn size and yarn spacing on the surface. The roll-off angles of these superhydrophobic surfaces were less than 5° when a large drop of water was applied, but greater than 5° when small drops were applied, since the roll-off angle was influenced by the droplet size and local yarn or fabric geometry.

7. PRODUCT DESIGN AND DEVELOPMENT

What is successful product design and development? Successful product design and development result in products that can be sold profitably. However, profitability is often difficult to evaluate quickly and directly. The following five specific dimensions related to profit can be used to evaluate the performance of product design and development: product quality, product cost, development time, development cost, and market feasibility. Since these present huge challenges for product designers, only a few companies are successful in their product development in high-tech product markets. In developing new high-tech textile products based on such excellent superhydrophobic materials or the surface modifying technologies introduced in this research, the product designer should search potential markets in which to apply the developed materials or technologies. For new high-tech product designs, the new materials or technologies should fit easily into existing products or processes. Therefore, new product development often uses modifications of generic materials to easily access the potential markets.

7.1. Production approach

Using the surface modifications presented in this research, many new products consisting of permanently durable self-cleaning textile fabrics can be designed. In order to access potential markets, a cost-effective, eco-friendly, continuous production method, which is applicable to mass production in the textile industry, needs to be developed. In this

work, low surface tension materials such as alkylamine as well as PAA were grafted onto the textile surfaces using a coupling agent, DMTMM. Since this coupling agent is expensive and not listed on the Toxic Substances Control Act (TSCA) list, the grafting method has to be modified. We can use padding to apply alkyl materials to the fabric surfaces followed by air-drying and high-temperature curing to graft the alkylamine onto the surfaces as shown in Figure 7.1.

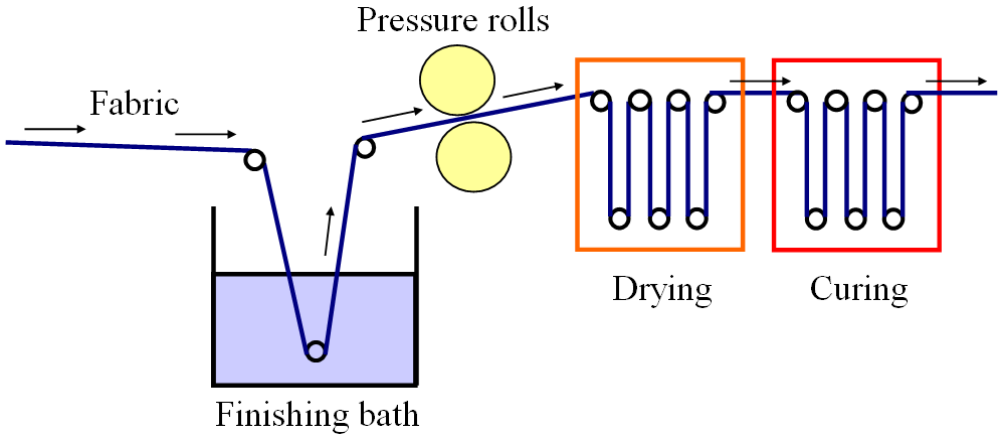

Figure 7.1. Padding process for cost-effective, eco-friendly, continuous production of superhydrophobic textile fabric.

Padding is a commonly used finishing process in textile mills due to its economics, efficiency and continuous production. In this process, a roll of textile fabric is dipped into an alkylamine solution, which wets the fabric, and the excess solution is removed by nip rollers. The fabric is dried in a tenter frame which blows warm-air onto the fabric. After it is dried, the temperature is raised to graft alkylamine to the fabric. It is expected that the textile surfaces prepared by this process will have the same contact angles and roll-off

angles as those of the alkylamine-grafted fabric made by our current process in which the coupling agent is used.

7.2. Market approach

Superhydrophobic textile fabrics developed in this research can be used as new platform products. Platform products are generally built near an existing technological system. The technology platform shown in the previous section has already demonstrated its usefulness in mass production and its huge potential for the existing markets as well as new markets. Therefore, product design built on technology platform is simpler than product design built on technology-push products. In designing a new technology-push product, a designer begins to work with a novel material or a unique technology to look for potential markets where the material or the technology can be applied. The potential markets for the new products consisting of self-cleaning surfaces are shown in Table 7.1.

Table 7.1. Potential markets and new products using self-cleaning technologies

Potential markets	Possible new products
Fashion and apparel	Self-cleaning outerwear, shoes, bags, cosmetics; Stain-release kids' wear, mechanics' uniform, etc.
Residential interiors and exteriors	Self-cleaning outdoor furniture, windows, roofs; Stain-release carpets, paint, wallpaper, etc.
Automotive interiors and exteriors	Self-cleaning auto glass, body shells, convertible tops
Biomedical textiles	Oil & water-release medical gown, stain-release bed clothes; Artificial organs such as blood vessel and scaffold, etc.

The product design cannot be successful if the technology does not offer a clear competitive advantage satisfying customer's needs. For example, stain-release kids' wear has to maintain soft hand, dimensional stability after 30 launderings, and colorfastness to saliva and perspiration. Self-cleaning convertible tops have to consist of coating materials having good durability after car washing, sunlight, and high or low temperature exposure. Self-cleaning roofs have to be well designed to enhance the Lotus effect while maintaining the original external appearance. Superhydrophobic-oleophobic surgical gowns need materials having appropriate softness, high thermal conductivity, and perspiration permeability. In developing artificial organs, it is important to design the new products while considering the biocompatibility for their applications. Therefore, the prototype samples of new biotextile products have to be evaluated through *in vitro* and *in vivo* tests.

8. REFERENCES

[1] Wu, X.; Shi, G. *J. Phys. Chem. B*, **2006**, *110*, 11247.

[2] Barthlott, W.; Neinhuis, C. *Planta* **1997**, *202*, 1.

[3] Neinhuis, C.; Barthlott, W. *Annals of Botany* **1997**, *79*, 667.

[4] Tavana, H.; Amirafazli, A.; Neumann, W. *Langmuir* **2006**, *22*, 5556.

[5] Gao, L.; McCarthy, T. J. *Langmuir* **2006**, *22*, 2966.

[6] Nosonovsky, M.; Bhushan, B. *Microsyst. Tech.* **2006**, *12*, 231.

[7] Zhang, J.; Kwok, D. Y. *Langmuir* **2006**, *22*, 4998.

[8] Dupuis, A.; Yeomans, J. M. *Langmuir* **2005**, *21*, 2624.

[9] Lee, J.; He, B.; Patankar, N. A. *J. Micromech. Microeng.* **2005**, *15*. 591.

[10] Li, W.; Amirfazli, A. *J. Colloid and Interface Sci.* **2005**, *292*, 195.

[11] Zhang, X.; Sato, O.; Taguchi, M.; Einaga, Y.; Murakami, T.; Fujishima, A. *Chem Mater* **2005**, *17*, 696.

[12] Shirtcliffe, N. J.; McHale, G.; Newton, M. I.; Perry, C. C. *Langmuir* **2003**, *19*, 5626.

[13] Otten, A., Herminghaus, S. *Langmuir* **2004**, *20*, 2405.

[14] Fuerstner, R.; Barthlott, W.; Neinhuis, C.; Walzel, P. *Langmuir* **2005**, *21*, 956.

[15] Cassie, A. B. D.; Baxter, S. *Nature Lond.* **1945**, *155*, 21.

[16] Nicolas, M.; Guittard, F.; Geribaldi, S. *Langmuir* **2006**, *22*, 3081.

[17] Shastry, A.; Case, M. J.; Boehringer, K. F. *Langmuir* **2006**, *22*, 6161.

[18] Pal, S.; Weiss, H.; Keller, H.; Mueller-Plathe, F. *Langmuir* **2005**, *21*, 3699.

[19] Lau, K. K. S.; Bico, J.; Teo, K. B. K.; Chhowalla, M.; Amaratunga, G. A. J.; Milne, W. I.; McKinley, G. H.; Gleason, K. K. *Nano Lett.* **2003**, *3*, 1701.

[20] Kovats, E. *Pure and App Chem.* **1989**, *61*, 1937.

[21] Brar, T.; France, P.; Smirniotis, P. *J Phy. Chem B* **2001**, *105*, 5383.

[22] Pal, S.; Weiss, H.; Keller, H.; Mueller-Plathe, F. *Langmuir* **2005**, *21*, 3699.

[23] Balkenede, A. R.; Boogaard, H. J. A. P. van de; Scholten, M.; Willard, N. P. *Langmuir* **1998**, *14*, 5907.

[24] Fowkes, F. M. *J Phys Chem* **1963**, *67*, 2538.

[25] Ostrovskaya, L.; Podesta, A.; Milani, P.; Ralchenko, V. *Europhys Lett* **2003**, *63*, 401.

[26] Barton, A. F. M. *CRC Handbook of solubility parameters and other cohesion parameters*; CRC Press, Inc.: Boca Raton, FL, 1983.

[27] van Krevelen, D. W.; Hoftyzer, P. J. In Properties of Polymers; Elsevier/North-Holland: New York, 1980; Vol. 2, Chapter 8, pp 166-172.

[28] Lee, L. *Langmuir* **1996**, *12*, 1681.

[29] Alberti, G.; Desimone, A. *Proc. Roy. Soc. London A* **2004**, *461*, 79.

[30] Chow, T. S. *J. Phys.: Condens. Matter* **1998**, *10*, L445.

[31] Li, W.; Amirfazli, A. *Journal of Colloid and Interface Science* **2005**, *292*, 195.

[32] Hosono, E.; Fujihara, S.; Honma, I.; Zhou, H. *JACS Communications* **2005**, *127*, 13458.

[33] Bico, J.; Tordeux, C.; Quere, D. *Europhys Lett* **2001**, *55*, 214.

[34] Rosario, R.; Gust, D.; Garcia, A. A.; Hayes, M.; Taraci, J. L.; Clement, T.; Dailey, J. W.; Picraux, S. T. *J. Phys. Chem. B.* **2004**, *108*, 12640.

[35] Sun, M.; Luo, C.; Xu, L.; Ji, H.; Ouyang, Q.; Yu, D.; Chen, Y. *Langmuir* **2005**, *21*, 8978.

[36] Zheng, Q.; Yu, Y.; Zhao, Z. *Langmuir* **2005**, *21*, 12207.

[37] Yoshimitsu, Z.; Nakajima, A.; Watanabe, T.; Hashimoto, K. *Langmuir* **2002**, *18*, 5818.

[38] Sun, T.; Feng, L.; Gao, X.; Jiang, L. *Acc Chem Res* **2005**, *38*, 644.

[39] Kwong, V. H.; Mossman, M. A.; Whitehead, L. A. *App Optics* **2004**, *43*, 808.

[40] Cassie, A. B. D.; Baxter, S. *Trans. Faraday Soc.* **1944**, *40*, 546.

[41] Marmur, A. *Langmuir* **2003,** 19, 8343.

[42] Wu, X., Zheng, L., Wu, D. *Langmuir* **2005**, *21*, 2665.

[43] Zhao, X.; Jiang, P.; Xie, S.; Feng, J.; Gao, Y.; Wang, J.; Liu, D.; Song, L.; Liu, L.; Dou, X.; Luo, X.; Zhang, Z.; Xiang, Y.; Zhou, W.; Wang, G. *Nanotechnology* **2006**, *17*. 35.

[44] Krupenkin, T. N.; Taylor, J. A.; Schneider, T. M.; Yang, S. *Langmuir* **2004**, *20*, 3824.

[45] McHale, G.; Aqil, S.; Shirtcliffe, N. J.; Newton, M. I.; Erbil H. Y. *Langmuir* **2005**, *21*, 11053.

[46] Kim, J., Kim, C. *J Microelectromechanical System* **2002**, *11*, 454.

[47] Ma, M.; Mao, Y.; Gupta, M.; Gleason, K. K.; Rutledge, G. C. *Macromolecules* **2005**, *38*, 9742.

[48] Singh, A.; Steely, L.; Allcock, H. R. *Langmuir* **2005**, *21*, 11604.

[49] Vogelaar, L.; Lammertink, R. G. H.; Wessling, M. *Langmuir* **2006**, *22*, 3125.

[50] He. B.; Patankar, N. A.; Lee, J. *Langmuir* **2003**, *19*, 4999.

[51] Dupuis, A.; Yeomans, J. M. *Langmuir* **2005**, *21*, 2624.

[52] Patankar, N. A. *Langmuir* **2003**, *19*, 1249.

[53] Lee, J.; He, B.; Patankar, N. A. *Journal of Micromechanics and Microengineering* **2005**, 15, 591.

[54] Jeong, H. E.; Lee, S. H.; Kim, J. K.; Suh, K. Y. *Langmuir* **2006**, *22*, 1640.

[55] Patankar, N. A. *Langmuir* **2003**, *19*, 1249.

[56] Wang X. D.; Peng, X. F.; Lu, J. F.; T. Liu; Wang, B. X. *Heat Transfer-Asian Research* **2004**, *33*, 201.

[57] Barthlott, W.; Neihuis, C. *Planta* **1997**, *202*, 1.

[58] Dorrer, C.; Ruehe, J. *Langmuir* **2006**, *22*, 7652.

[59] Yoshimitsu, Z.; Nakajima, A.; Watanabe, T.; Hashimoto, K. *Langmuir* **2002**, *18*, 5818.

[60] Brandon, S.; Haimovich, N.; Yeger, E.; Marmur, A. *J. Colloid and Interface Sci.* **2003**, *263*, 237

[61] Hennig, A.; Eichhorn, K. J.; Staudinger, U.; Sahre, K.; Rogalli, M.; Stamm, M.; Neumann, A. W.; Grundke, K. *Langmuir* **2004**, *20***,** 6685.

[62] Miwa, M.; Nakajima, A.; Fujishima, A.; Hashimoto, K.; Watanabe, T. *Langmuir* **2004**, *16*, 5754.

[63] Roura, P.; Fort, J. *Langmuir* **2002**, *18*, 566.

[64] McHale, G.; Shirtcliffe, N. J.; Newton, M. I. *Langmuir* **2004**, *20*, 10146.

[65] Zhu, M.; Zuo, W.; Yu, H.; Yang, W.; Chen, Y. *J. Mater. Sci.* **2006**, *41*, 3793.

[66] Gao, L.; McCarthy, T. J. *Langmuir* **2006**, *22*, 5998.

[67] Lee, H. J.; Michielsen, S. *J. Polym. Sci. Part B: Polym. Phys.* **2007**, *45*, 253.

[68] Jopp, J.; Gruell, H.; Yerushalmi-Rozen, R. *Langmuir* **2004**, *20*, 10015.

[69] Lau, K. K. S.; Bico, J.; Teo, K. B. K.; Chhowalla, M.; Amaratunga, G. J.; Milne, W. I.; McFinley, G. H.; Gleason, K. K. *Nano Lett.* **2003**, *3*, 1701.

[70] Nakajima, A.; Hashimoto, K.; Watanabe, T. *Langmuir* **2005**, *16*, 7044.

[71] Zhai, L.; Cebeci F. C.; Robert, E. C.; Rubner, M. F. *Nano Lett* **2004**, *4*, 1349.

[72] Han, J. T.; Xu, X.; Cho, K. *Langmuir* **2005**, *21*, 6662.

[73] Huang, L.; Lau, S. P.; Yang, H. Y.; Leong, E. S. P.; Yu, S. F. *J. Phys. Chem B.* **2005**, *109*, 7746.

[74] Shang, H. M.; Wang, Y.; Limmer, S. J.; Chou, T. P.; Takahashi, K.; Cao, G. Z. *Thin Solid Films* **2005**, *472*, 37.

[75] Shi, F.; Song, Y.; Niu, J.; Xia, X.; Wang, Z.; Zhang, X. *Chem. Mater.* **2006**, *18*, 1365.

[76] Jeong, H. E., Lee, S. H., Kim, J. K., Suh, K. Y. *Langmuir* **2006**, *22*, 1640.

[77] Kim, S. H.; Kim, J.; Kang, B.; Uhm, H. *Langmuir* **2005**, *21*, 12213.

[78] Fresnais, J.; Chapel, J. P.; Poncin-Epailard, F. *Surface & Coating Technology* **2006**, *200*, 5296.

[79] Baumann, M.; Fritsche, K.; Korbelarz, D.; Ludwig, S.; Poth, L. U.S. Patent Application 20,020,142,150, 2002.

[80] Baumann, M.; Fritsche, K.; Korbelarz, D.; Ludwig, S.; Poth, L. U.S. Patent Application 20,050,170,098, 2005.

[81] Buchsel, M.; Kaussen, M.; Schroft, S. U.S. Patent Application 6,712,932, 2004.

[82] Kaibel, G.; Domschke, T.; Haake, M.; Keller, H.; Schwab, E.; Oost, C. U.S. Patent Application 20,040,023,798, 2004.

[83] Nun, E.; Oles, M. U.S. Patent Application 20,030,147,932, 2003.

[84] Nun, E.; Oles, M.; Lang, A. U.S. Patent Application 20,050,112,326, 2005.

[85] Wang, M. U. S. Patent Application 20,050,112,359, 2005.

[86] BASF, www.corporate.basf.com/en/presse/fotos/-pfasset.htm?aid=1015&sprache=en&id=6TFfX7Hzdbcp4Re

[87] BASF, www.basf.de/basf/img/futurebusiness/Flyer_mincor.pdf

[88] BASF, www.corporate.basf.com/en/innovationen/felder/nanotechnologie/fotos/?id=V00-J9RZY7Hz8bcp.h8

[89] Nanotex, www.nano-tex.com/news&media/Star_Tribune_12-4-04.pdf

[90] Nanotex, www.nano-tex.com/news&media/popscience_Mar-2005.pdf

[91] Nanotex, www.nano-tex.com/products/spills_info.pdf

[92] Thompson, K. F. Ph.D. Dissertation, Georgia Institute of Technology, Atlanta, GA, 2005.

[93] Tobiesen, F. A.; Michielsen, S. *J Polym Sci Part A: Polym Chem*, **2002**, *40*, 719.